The Pennsylvania State University
APPLIED RESEARCH LABORATORY
P.O. Box 30
State College, PA 16804

CALCULATION OF TURBULENT BOUNDARY LAYER WALL PRESSURE SPECTRA

by

D. E. Capone
Naval Surface Warfare Center
Acoustic Research Detachment
Code 752
P.O. Box 129
Bayview, ID 83803-0129

G. C. Lauchle
The Pennsylvania State University
Applied Research Laboratory

Technical Report No. TR 93-10
August 1993

Supported by:
Naval Surface Warfare Center

L.R. Hettche, Director
Applied Research Laboratory

REPORT DOCUMENTATION PAGE

Form Approved
OMB No. 0704-0188

1. AGENCY USE ONLY (Leave blank)	2. REPORT DATE	3. REPORT TYPE AND DATES COVERED
	August 1993	

4. TITLE AND SUBTITLE

CALCULATION OF TURBULENT BOUNDARY LAYER WALL PRESSURE SPECTRA

5. FUNDING NUMBERS

6. AUTHOR(S)

Dean E. Capone and G. C. Lauchle

7. PERFORMING ORGANIZATION NAME(S) AND ADDRESS(ES)

Naval Surface Warfare Center
Acoustic Research Detachment
Code 752
P.O. Box 129
Bayview, ID 83803-0129

8. PERFORMING ORGANIZATION REPORT NUMBER

TR-93-10

9. SPONSORING/MONITORING AGENCY NAME(S) AND ADDRESS(ES)

Naval Surface Warfare Center
Acoustic Research Detachment
Code 752
P.O. Box 129
Bayview, ID 83803-0129

10. SPONSORING/MONITORING AGENCY REPORT NUMBER

11. SUPPLEMENTARY NOTES

12a. DISTRIBUTION/AVAILABILITY STATEMENT

Unlimited

12b. DISTRIBUTION CODE

13. ABSTRACT *(Maximum 200 words)*

This study is an investigation into the suitability of various wavevector-frequency models of turbulent boundary layer wall pressure fluctuations for the prediction of experimental measurements of turbulent boundary layer wall pressure spectra. Three separate models of the wavevector-frequency spectrum proposed by D. M. Chase in 1980 and 1987 are evaluated. The wavevector-frequency spectral models are integrated numerically using a formulation for the point wall pressure spectrum (based on the work of Uberoi and Kovasznay). The representation of the wall pressure spectrum used accounts for the effect of a finite sized transducer on the measured wall pressure spectrum. By accounting for the area averaging effect of finite sized transducers on the measured turbulent boundary layer wall pressure spectra, it was possible to use Chase's rigorous formulations for the wavevector-frequency spectrum instead of the point pressure spectrum representations which assume an infinitely small measurement sensor.

Results from the numerical integrations are compared to recent experimental data to determine which model of the wavevector-frequency spectrum most accurately predicts measured turbulent boundary layer wall pressure spectra. Data from experiments using fluids with a wide range of physical properties (air, water, and glycerine) are used for comparison purposes. Using the selected model, new empirical constants are established for use in the model for each fluid under consideration. Justification for use of the new empirical constants is given, and current limitations of the wavevector-frequency models are discussed.

14. SUBJECT TERMS

turbulent boundary layer, wall, pressure spectra, wavevector, chase

15. NUMBER OF PAGES

69

16. PRICE CODE

17. SECURITY CLASSIFICATION OF REPORT	18. SECURITY CLASSIFICATION OF THIS PAGE	19. SECURITY CLASSIFICATION OF ABSTRACT	20. LIMITATION OF ABSTRACT
Unclassified	Unclassified	Unclassified	

ABSTRACT

This study is an investigation into the suitability of various wavevector-frequency models of turbulent boundary layer wall pressure fluctuations for the prediction of experimental measurements of turbulent boundary layer wall pressure spectra. Three separate models of the wavevector-frequency spectrum proposed by D. M. Chase in 1980 and 1987 are evaluated. The wavevector-frequency spectral models are integrated numerically using a formulation for the point wall pressure spectrum (based on the work of Uberoi and Kovasznay). The representation of the wall pressure spectrum used accounts for the effect of a finite sized transducer on the measured wall pressure spectrum. By accounting for the area averaging effect of finite sized transducers on the measured turbulent boundary layer wall pressure spectra, it was possible to use Chase's rigorous formulations for the wavevector-frequency spectrum instead of the point pressure spectrum representations which assume an infinitely small measurement sensor.

Results from the numerical integrations are compared to recent experimental data to determine which model of the wavevector-frequency spectrum most accurately predicts measured turbulent boundary layer wall pressure spectra. Data from experiments using fluids with a wide range of physical properties (air, water, and glycerine) are used for comparison purposes. Using the selected model, new empirical constants are established for use in the model for each fluid under consideration. Justification for use of the new empirical constants is given, and current limitations of the wavevector-frequency models are discussed.

TABLE OF CONTENTS

LIST OF FIGURES

LIST OF SYMBOLS

b	Scale Coefficient
c	Speed of sound in fluid
d^+	Transducer diameter in viscous wall units, du_*/υ
$G_{TT}(\omega)$	Autospectrum of turbulent boundary layer
h	Velocity Dispersion Coefficient
$\lvert H(k_1, k_3)\rvert^2$	In-plane wavenumber response of sensor
$\mathbf{k} = (k_1, k_3)$	Shorthand notation for in-plane wavenumber
k_1	Wavenumber in x_1 direction
k_2	Wavenumber in x_2 direction
k_3	Wavenumber in x_3 direction
k_c	Convective wavenumber
$K=(k_1^2 + k_3^2)^{1/2}$	Magnitude of in-plane wavevector
$P(\omega)$	Point pressure spectrum
$P(k_1,k_3,\omega)$	Wavenumber-frequency spectrum
$P(\mathbf{k},\omega)$	Shorthand notation for the wavenumber-frequency spectrum
R	Space-time correlation function
Re	Reynolds number
Rh	Channel Reynolds number
Re_θ	Reynolds number with respect to momentum thickness
$S(x_3,x_3',k,\omega)$	Cross-spectral density of fluctuating velocities
u,v,w	Velocities in x_1,x_2,x_3 directions respectively
$\bar{u}$	Time averaged velocity component
u'	Fluctuating velocity component
u_*	Friction velocity

U_{av}	Pipe flow average velocity
U_c	Convective velocity
x_1, x_2, x_3	Orthogonal coordinate system
x_2^+	Non-dimensionalized distance from the wall, $x_2 u_* / \upsilon$

Greek Symbols

δ	Boundary layer thickness
μ	Viscosity of fluid
ρ	Density of fluid
θ	Momentum thickness
υ	Kinematic viscosity of fluid
τ'_{ij}	Reynold's stress tensor
τ_w	Wall shear stress

Chapter 1

INTRODUCTION

Wall pressure fluctuations beneath turbulent boundary layers have been of interest to scientists and engineers for many years. Willmarth[1] gives one of the best summaries of our understanding of the physics involved with pressure fluctuations under turbulent boundary layers, prior to 1975. In the past, the work performed on wall pressure fluctuations has been focused in two areas - experimental investigation and theoretical prediction. A thorough understanding of pressure fluctuations beneath turbulent boundary layers has importance in many fields, such as underwater sonar applications and aircraft cabin noise. Due to the efficient coupling between underwater structures and energy in the low wavenumber region of the turbulent boundary layer, this region of the boundary layer wall pressure spectrum is of particular interest.

Until recent advances in the areas of sensor technology and signal processing, the accurate measurement of boundary layer pressure fluctuations had proved difficult. Low frequency components of the turbulent boundary layer were often masked by the noise of the measurement facility. Often times, due to the large size of the pressure transducers employed, the high frequency components were not measured correctly. The large pressure transducers resulted in area averaging over the face of the transducer. The area averaging lowers the measured level of the high frequency components. Since the established theoretical models relied upon experimental data for implementation, the accuracy of these models was affected. The recent advances in sensor technology and signal processing have provided better estimates of the pressure spectrum of the turbulent boundary layer than were previously available. Examination of the recent experimental results has led to changes in precious theoretical models. Armed with new theoretical

models, it should now be possible to more accurately predict the turbulent boundary layer wall pressure spectrum.

A review of boundary layer theory is provided in Chapter 2. The source of the turbulent boundary layer pressure fluctuations is seen to be the fluctuating velocities that occur in the boundary layer, and Poisson's equation, which relates the fluctuating velocities to fluctuating pressure, is derived. Finally, the two contributions to the measured wall pressure spectra are identified as the mean shear-turbulence interaction term, and the turbulence-turbulence interaction term.

Once the equation relating fluctuating velocities to the fluctuating pressures has been derived, a review of contemporary models of the wavevector-frequency spectrum is provided. Chapter 3 begins with the equation which will be used to calculate the wall pressure spectra once a model of the wavevector frequency spectrum is established. This equation includes a factor which accounts for the in-plane wavenumber response of the circular transducers used to make the experimental measurements. A discussion of the early efforts to model the turbulent boundary layer wavevector-frequency spectrum is provided. Based on recent experimental measurements, changes to the older models of wavevector-frequency spectrum are discussed.

The greatest aid to revising the older models of the wavevector-frequency spectrum are more accurate measurements of the turbulent boundary layer wall pressure fluctuations. Results from three recent experiments are presented in Chapter 4. Advances in signal processing now enable an investigator to post-process acquired data and remove much of the facility noise contamination. Results from two experiments, performed in glycerine and water, where such techniques have been used are presented. All three experiments

discussed also employed extremely small pressure sensors which allow for more accurate resolution of the high frequency components of the turbulent boundary layer wall pressure fluctuations.

The techniques used to numerically integrate the double integral, presented in Chapter 3, which yields the calculated wall pressure spectrum, are discussed in Chapter 5. The integrals are evaluated by the use of a two-dimensional Simpson's rule. All parameters used for the integrations are presented, including the empirical constants from the wavevector-frequency models.

Chapter 6 presents the results of the numerical integrations. Calculated results are compared to the actual measurements. Next, the effect of the empirical constants in the wavevector-frequency model are explored. Using the information gained, the constants are adjusted to provide a better fit to the measured data. The results of the integrations are discussed in Chapter 7. Explanations as to why new empirical constants were needed are presented. Lastly, recommendations for future work are included.

Chapter 2

BACKGROUND

2.1 Boundary Layer Theory

As a body moves through a fluid, the flow characteristics of a thin region of the fluid located near the surface of the body are affected by the viscosity of the fluid. The region where the viscosity of the fluid is an important flow parameter is termed the boundary layer. As an example, Figure 1 illustrates the mean velocity distribution in a boundary layer on a flat plate.

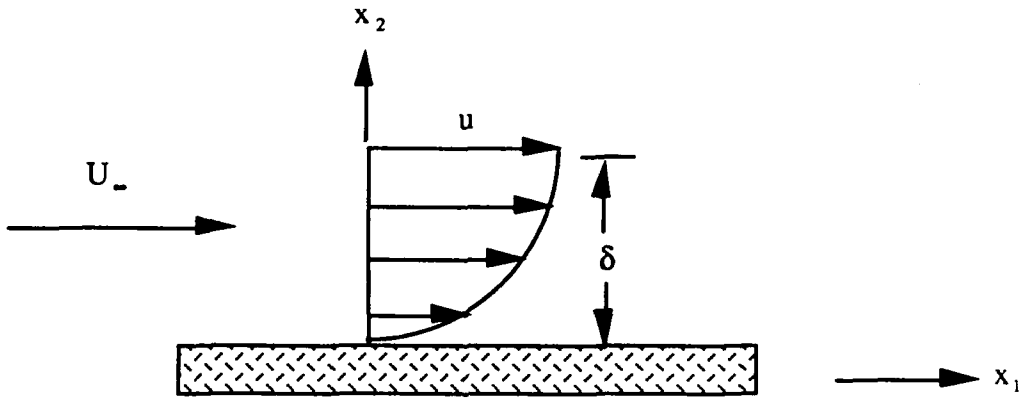

Figure 1 - Boundary Layer Mean Velocity Profile

Due to the viscosity of the fluid, the velocity at the wall is zero; this is termed the no-slip condition. As a result of the zero velocity at the wall, the velocity gradient, $\partial u/\partial x_2$, near the wall is large. Variation of flow field in the x_3 direction, taken to be out of the plane of the page, is considered negligible. The boundary layer thickness, δ, is defined as the distance from the wall where the velocity in the x_1 direction, u, reaches .99 U_∞, where U_∞

is the free stream velocity.[2]

As a result of the velocity gradient, $\partial u/\partial x_2$, being large within the boundary layer, the normal wall shear stress

$$\tau_w = \mu \left. \frac{\partial u}{\partial x_2} \right|_{x_2=0}, \tag{2.1}$$

where μ is the viscosity of the fluid, becomes an important parameter. Equation 2.1 is known as Newton's Law of friction. Within the boundary layer, friction and inertia forces are of comparable magnitude.[3]

The Reynolds number,

$$Re = \frac{\rho U_\infty x_1}{\mu}, \tag{2.2}$$

where ρ is the density of the fluid and x_1 is the streamwise wetted length, is the quantity used for determination of the dynamic similarity of boundary layer flows. Ignoring the effects of elastic and gravitational forces, the Reynolds number can be considered the ratio of inertial forces to frictional forces. As stated above, within turbulent boundary layers, the frictional and inertial forces are of comparable magnitude. Using the Reynolds number, the wall shear stress for turbulent flow over a smooth flat plate can be approximated by

$$\tau_w = 0.029 \rho U_\infty^2 \, Re^{-1/5}. \tag{2.3}$$

As the Reynolds number of a flow increases, transition will occur from a laminar

boundary layer to a turbulent boundary layer. A laminar boundary layer flow is characterized by smooth and steady flow in the direction along the surface. Only small velocity fluctuations normal to the flow direction occur around a mean value of flow velocity within a laminar boundary layer. As the flow transitions from laminar to turbulent, velocity fluctuations within the boundary layer become pronounced. These velocity fluctuations can range up to 50% of the mean flow velocity.[3] As a result of the dramatic velocity fluctuations within a turbulent boundary layer, the pressure at a given point also fluctuates with time.

2.1.1 TURBULENT FLOW

Due to the random nature of the velocity fluctuations within a turbulent boundary layer, statistical methods must be used to describe the flow. In three dimensional turbulent flow, the velocities and pressure are functions of all three spatial variables and time, e.g.

$$u = u(x_1, x_2, x_3, t). \tag{2.4}$$

The theoretical models examined in this paper consider only turbulent flow over a smooth, rigid plane without a pressure gradient. The flow is assumed to be homogeneous in the plane of the wall; therefore, two-dimensional flow will be considered. In order to model the pressure and velocity within a turbulent boundary layer, the quantities are represented by their mean and fluctuating components

$$u = \bar{u} + u' \quad v = \bar{v} + v' \quad p = \bar{p} + p', \tag{2.5}$$

where $\bar{u}$ is the time average of the velocity in the x_i direction and u' is the fluctuating

velocity about $\bar{u}$. The time average of a fluctuating quantity is defined as having a zero mean value.

The influence of the fluctuating components of velocity on the mean flow results in an apparent increase in viscosity of the fluid. Such effects manifest themselves as a stress field throughout the turbulent layer. These stresses are called Reynolds stresses; for two-dimensional flow the stress tensor is[3]:

$$\tau'_{ij} = \begin{pmatrix} \sigma'_x & \tau'_{xy} \\ \tau'_{xy} & \sigma'_y \end{pmatrix} = -\rho \begin{pmatrix} \overline{u'^2} & \overline{u'v'} \\ \overline{u'v'} & \overline{v'^2} \end{pmatrix}. \qquad (2.6)$$

In turbulent flow, these Reynolds stresses act on the fluid in addition to the wall shear stress, Equation (2.3), which is the dominant factor in laminar flow.

The turbulent boundary layer on a rigid surface is considered to be composed of three regions. As one progresses away from the wall in the x_2 direction, the first region, the viscous sub-layer, is an extremely thin region near the surface where all components of the stress tensor are very small. In this region, the viscous stresses, Equation (2.3), dominate the flow. The viscous sub-layer is sometimes referred to as the laminar sub-layer since the flow is dominated by viscous stresses. The second region, the buffer or overlap layer, is an area where the viscous and Reynolds stresses are of a comparable order of magnitude. In the third region, the inertial sub-layer, the flow is dominated by the Reynolds stresses.[4] The viscous sub-layer is also commonly referred to as the inner layer, while the inertial sub-layer is often referred to as the outer layer.

The friction velocity:

$$u_* = \sqrt{\frac{\tau_w}{\rho}}, \tag{2.7}$$

is representative of the shear velocities present very close to the wall in turbulent flow. Length and velocity scales in turbulent flows are typically non-dimensionalized by use of u_* and υ, where υ is the kinematic viscosity:

$$\upsilon = \frac{\mu}{\rho}. \tag{2.8}$$

Using the friction velocity and the kinematic viscosity, the inner variable , x_2^+, is defined as:

$$x_2^+ = \frac{x_2 u_*}{\upsilon}. \tag{2.9}$$

White[5] defines the overlap layer as between $35 \le x_2^+ \le 350$ with the outer layer at $x_2^+ \ge 350$.

2.2 POISSON'S EQUATION

To determine the wall pressure spectrum due to the turbulent boundary layer, the relationship between the fluctuating velocities and pressure must be defined. Following the example of Kraichnan[6] and Blake[7], one begins with the equation of continuity

$$\frac{\partial \rho}{\partial t} + \frac{\partial (\rho u_i)}{\partial x_i} = 0, \tag{2.10}$$

and the momentum equation

$$\rho \frac{\partial u_i}{\partial t} + \rho u_j \frac{\partial u_i}{\partial x_j} + \frac{\partial p}{\partial x_i} - \upsilon \nabla^2 u_i = 0, \tag{2.11}$$

where i and j=1,2 for two dimensional incompressible flow. Differentiating Equation (2.11) with respect to x_i and Equation (2.10) with respect to time, and subtracting the results, one obtains:

$$\frac{\partial^2 p}{\partial x_i^2} = -\rho \frac{\partial^2 (u_i u_j)}{\partial x_i \partial x_j}. \tag{2.12}$$

Next, following the work of Farabee[8], the pressure and velocities are replaced by their mean and fluctuating quantities, Equation (2.5), which yields:

$$\frac{\partial^2 \overline{p}}{\partial x_i^2} + \frac{\partial^2 p'}{\partial x_i^2} = -\rho \frac{\partial^2}{\partial x_i \partial x_j} \left(\overline{u}_i \overline{u}_j + \overline{u}_i u_j' + u_i' \overline{u}_j + u_i' u_j' \right). \tag{2.13}$$

Taking a time average of Equation (2.13) eliminates the linear fluctuating quantities leaving

$$\frac{\partial^2 \overline{p}}{\partial x_i^2} = -\rho \frac{\partial^2}{\partial x_i \partial x_j} \left(\overline{u}_i \overline{u}_j + \overline{u_i' u_j'} \right). \tag{2.14}$$

Substituting Equation (2.14) back into Equation (2.13) yields:

$$\frac{\partial^2 p'}{\partial x_i^2} = -\rho \frac{\partial^2}{\partial x_i \partial x_j}\left(2\bar{u}_i u_j' + u_i' u_j' - \overline{u_i' u_j'}\right). \tag{2.15}$$

Noting that $\nabla \circ \bar{u} = 0$, then

$$\frac{\partial}{\partial x_i x_j}(2\bar{u}_i u_j') = 2\frac{\partial \bar{u}_i}{\partial x_j}\frac{\partial u_j'}{\partial x_i};$$

and rearrangement of the first term on the right hand side of Equation (2.15) yields:

$$\frac{\partial^2 p'}{\partial x_i^2} = -\rho\left\{2\frac{\partial u_i}{\partial x_j}\frac{\partial u_j'}{\partial x_i} - \frac{\partial^2}{\partial x_i \partial x_j}\left(u_i' u_j' - \overline{u_i' u_j'}\right)\right\}. \tag{2.16}$$

For two-dimensional boundary layer flow, the mean velocity is assumed to be a function of the x_2 direction only; while the fluctuating velocities are considered a function of both the x_1 and x_2 directions. With these assumptions, Equation (2.16) reduces to the Poisson equation for the unsteady pressure:

$$\frac{\partial^2 p'}{\partial x_i^2} = -\rho\left\{2\frac{\partial u_1}{\partial x_2}\frac{\partial u_2'}{\partial x_1} - \frac{\partial^2}{\partial x_i \partial x_j}\left(u_i' u_j' - \overline{u_i' u_j'}\right)\right\}. \tag{2.17}$$

As first noted by Kraichnan the first term on the right-hand side of Equation (2.17) represents the interaction of the mean shear (See Equation 2.1) in the flow, with the turbulence. The second term on the right-hand side of the equation represents the turbulence-turbulence interaction. Equation (2.17) shows that the fluctuating velocities within the turbulent boundary layer are the source of the pressure fluctuations generated by the boundary layer. As will be seen in later sections, if one can adequately model the

fluctuating velocities within the various turbulent boundary layer regions, a reasonable estimate of the wall pressure spectrum can be obtained.

Chapter 3

MODELING THE TURBULENT BOUNDARY LAYER WALL PRESSURE SPECTRUM

3.1 Autospectrum of the Turbulent Boundary Layer Wall Pressure Fluctuations

Based on the work of Uberoi and Kovasznay[9] and in the notation of Lauchle[10], the autospectrum of the turbulent boundary layer wall pressure fluctuations is given by:

$$G_{TT}(\omega) = 2\int_{-\infty}^{\infty}\int_{-\infty}^{\infty} P(k_1,k_3,\omega)\left|H(k_1,k_3)\right|^2 dk_1 dk_3, \tag{3.1}$$

where $P(k_1,k_3,\omega)$ is the wavenumber frequency spectral density of the turbulent boundary layer wall pressure fluctuations, and $\left|H(k_1,k_3)\right|^2$ is the in-plane wavenumber response of the measurement sensor. Equation (3.1) assumes the pressure fluctuations are acting directly on the face of a single transducer. The wavenumber response function accounts for area averaging of the pressure spectrum that results from a finite sized transducer. The wavenumbers result from the spatial Fourier transforms of the fluctuating wall pressure field. The wavevector in the plane of the wall is:

$$K = (k_1^2 + k_3^2)^{1/2}, \tag{3.2}$$

where k_1 is the flow direction wavenumber and k_3 is the cross-stream wavenumber. The in-plane wavenumber response for a circular transducer is given by

$$\left|H(KR)\right|^2 = \left[2J_1(KR)/KR\right]^2, \tag{3.3}$$

where R is the active radius of the sensing element, J_1 is a Bessel function of the first kind of order one, and $\mathbf{k} = (k_1, k_3)$ is a shorthand notation for the in-plane wavevector.

Using the above formulation for the autospectrum of the turbulent boundary layer, the sound pressure levels under a turbulent boundary layer can be calculated given $P(\mathbf{k},\omega)$. The form of the wavevector-frequency spectrum of the turbulent boundary layer has been the subject of extensive studies over the years and, as will be seen in the next section, $P(\mathbf{k},\omega)$ can be modeled in many different ways.

3.2 Wavevector-Frequency Spectrum

Some of the earliest work performed on modeling the wavevector-frequency spectrum was by Kraichnan[6]. Kraichnan identified two sources to the wall pressure spectrum; the interaction of the turbulence with the mean shear, and the turbulence interaction with itself--termed the turbulence-turbulence contribution. Based on his model of the boundary layer, Kraichnan estimated that the contribution of the turbulence-mean shear interaction term to the pressure spectrum was considerably more important than the turbulence-turbulence term. Figure 2 illustrates the wavenumber frequency spectrum of low Mach number turbulent wall pressure fluctuations as a function of streamwise wavenumber, k_1, for a fixed frequency ω. The majority of the energy is concentrated in what is termed the convective region. This region is centered on the convective wavenumber, $k_c = \omega/U_c$, where U_c is known as the convection velocity. The convection velocity is the speed at which the large scale eddies within the turbulent boundary layer travel. The convection velocity ranges typically between 0.5-0.7 U_∞.[11]

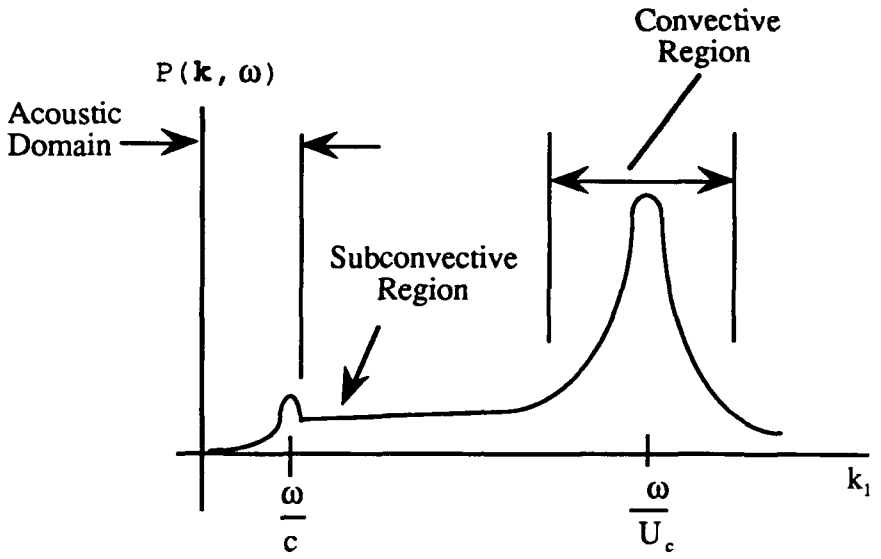

Figure 2 - Typical Form of the Wavenumber Frequency Spectrum of the Turbulent Boundary Layer Wall Pressure Fluctuations

The acoustic region is defined where $k_1 \leq \omega/c$, where c is the speed of sound in the fluid under consideration. In the past, most theoretical work concentrated on the convective region and very little information was available regarding the subconvective and acoustic regions.

3.2.1 Chase's 1980 Model

Modeling the subconvective or low wavenumber region of the turbulent boundary layer has proven to be a very complex and unresolved task. This is partially due to a lack of experimental data for this region and partially due to the fact that most of the energy in the boundary layer is concentrated in the convected region. Chase[12] published a paper in 1980 that included a model of the wavevector frequency spectrum for the incompressible, inviscid domain which includes convective and subconvective wavenumbers. Chase defines the region of subconvective wavenumbers, or the low wavenumber tail, as

$\omega/c << K << (\omega - uk_1)/3u_*$. The flow under consideration in this paper is a homogeneous turbulent boundary layer flow at low Mach number over a smooth, stationary, rigid plane with zero pressure gradient.

Chase's development follows that of Kraichnan[6] and is well summarized by Howe.[11] Chase defined $P(\mathbf{k},\omega)$ as the Fourier transform of the space-time correlation of the wall pressure:

$$P(\mathbf{k},\omega) = \frac{1}{(2\pi)^3}\iiint_{-\infty}^{\infty} R(y_1,y_3,\tau) \times \exp[-i(\mathbf{k}\mathbf{y} - \omega\tau)]dy_1 dy_3 d\tau , \tag{3.4}$$

where

$$R(y_1,y_3,t) = \langle p'(x_1,x_3,t)p'(x_1+y_1,x_3+y_3,t+\tau)\rangle, \tag{3.5}$$

is the space time correlation function of the fluctuating pressure, and the brackets represent ensemble averaging (see for example[13]). Given Equation (3.4), $R(y_1,y_3,t)$ can also be defined as the inverse Fourier transform of $P(\mathbf{k},\omega)$. The point pressure spectrum, $P(\omega)$, is defined as the pressure spectrum that would be measured by a sensor small enough so that no area averaging took place over the face of the sensor. The point pressure spectrum can be represented at a given frequency by

$$P(\omega) = \int_{-\infty}^{\infty}\int_{-\infty}^{\infty} P(\mathbf{k},\omega)dk_1 dk_3, \tag{3.6}$$

since $|H(KR)|^2 = 1.0$ for an infinitely small transducer (see Equation (3.3)).

Chase begins his effort to model the wavevector-frequency spectrum with two basic assumptions: $P(\mathbf{k},\omega)$ should tend to zero as K approaches zero, with functional form $P(\mathbf{k},\omega) \propto K^2$. For $K >> \omega/c$, the most general form for the wavevector-frequency spectrum is

$$P(\mathbf{k},\omega) = \rho^2 u_*^6 \omega^{-3} f\left(\frac{u_*\mathbf{k}}{\omega}, \mathbf{k}\delta, \frac{\omega\upsilon}{u_*^2}\right), \tag{3.7}$$

where it is assumed that dependence on Reynolds number was weak enough to be ignored. As suggested by Kraichnan[6], the total wavenumber-frequency spectrum is considered to be

$$P(\mathbf{k},\omega) = P_T(\mathbf{k},\omega) + P_M(\mathbf{k},\omega), \tag{3.8}$$

where $P_T(\mathbf{k},\omega)$ is the turbulence-turbulence interaction contribution, and $P_M(\mathbf{k},\omega)$ is the turbulence-mean shear interaction contribution. The convective region is assumed to be dominated by the turbulence-mean shear term, and the low wavenumber region by the turbulence-turbulence term.

One important point to note is that the model does not include the viscous domain, which is characterized by the viscous variable $\omega\upsilon/u_*^2$ in Equation (3.7). Chase points out that as long as $\omega\upsilon/u_*^2 \leq 2$, the effect of the viscous domain on the convective ridge will be small; and as long as $\omega\upsilon/u_*^2 \leq 1/2$, the effect on the low wavenumber region will be small.

In order to formulate his final model Chase relies on experimental data. He has noted that the results from the experiments may only bound the levels within the low wavenumber region and not be true measurements of the level. This is due to the difficulty

in measuring the relatively low pressure levels in the low wavenumber region as compared to the high levels found in the convective region. The final form that Chase[12] proposes for the wavevector-frequency spectrum [Equations (68) and (69) in his paper] is

$$P(\mathbf{k},\omega) = \rho^2 u_*^3 (C_M k_1^2 K_M^{-5} + C_T K^2 K_T^{-5}), \tag{3.9}$$

where

$$K_i^2 = (\omega - U_c k_1)^2 / h_i^2 u_*^2 + K^2 + (b_i \delta)^2;\ i = M,T. \tag{3.10}$$

In Equation (3.10), M indicates the turbulence-mean shear component; T indicates the turbulence-turbulence contribution; and δ, the boundary layer thickness, is defined as shown in Figure 1. One can see by examining Equation (3.9) that the resulting model is quadratic in wavenumber.

The model contains six dimensionless coefficients: C_M, C_T, b_M, b_T, h_M, and h_T; which must be determined by fitting the model to experimental data. The constants h_M and h_T, termed the velocity dispersion coefficients, arise from the longitudinal cross-spectral densities. An approximate value for b_M, the mean shear scale parameter, was determined by matching the maximum value of $P_M(\omega)$, as predicted by the model to the maximum value of $P(\omega)$ measured by experiment. An estimate for b_T, the turbulence-turbulence scale parameter, is obtained from the low frequency limit of $P(\omega)$; however the values are questionable due to the reliability of available low frequency data. For C_M, C_T, h_M and h_T, equations are given to calculate their values:

$$h_i = \frac{\mu_i U_c}{u_*};\ i = M,T \text{ and}$$

$$C_T = \frac{3r_T a_+}{2\pi h_T} \quad C_M = \frac{3r_M a_+}{2\pi h_M}, \tag{3.11}$$

where a_+ and r_T, the mixture coefficient, are determined from experimental data, and $r_M = 1 - r_T$.

Chase uses the data from Bull[14] to establish a set of values for the needed dimensionless coefficients:

$$\begin{aligned} a_+ &= 0.766,\ r_T = 0.389,\ b_M = 0.756 \\ b_T &= 0.378,\ \mu_M = \mu_T = 0.176\ , \end{aligned} \tag{3.12}$$

and compares the predicted results to the experimental results of Bull. The results of the model, Equations (3.9) and (3.10), with the indicated parameter set of Equation (3.12) agree well with Bull's data.

3.2.2 Chase's 1987 Model

In 1987, Chase[15] formulated a model for the wavevector-frequency spectrum which attempted to characterize $P(\mathbf{k},\omega)$ from the convective domain down into the acoustic domain. When considering the acoustic domain, some effects of compressibility of the fluid are taken into consideration.

In the paper he wrote in 1980, Chase assumed that $P(\mathbf{k},\omega)$ would tend to zero as K went to zero as a function of K^2. In this paper, the restrictions on the form of $P(\mathbf{k},\omega)$ in

the low wavenumber region are not as severe, and consideration is given to functional forms which may vary between K^0 to K^2. The result is a wall pressure spectrum that is termed wavevector-white, i.e. the level of the wall pressure is assumed constant for $K \leq (b\delta)^{-1}$ in the subconvective domain, where b is once again a scale factor. In the region $\omega/c \leq K \leq (b\delta)^{-1}$, the 1987 model is similar to the 1980 model in that $P(\mathbf{k},\omega)$ varies as K^2.

The development of the model proceeds upon lines very similar to those used in Chase's 1980 paper. Source spectra for the turbulence-turbulence interaction and the turbulence-mean shear interaction are obtained from the Fourier transform of the Poisson equation for unsteady pressure, Equation (2.17). As an example, the source spectrum for the turbulence-turbulence interaction term, P_T, is $S(x_2, x_2', \mathbf{k}, \omega)$; which is a sum of cross-spectral densities of fluctuating velocity products at positions x_2 and x_2', and is assumed to be of the form

$$S(x_2, x_2', \mathbf{k}, \omega) = \exp[-(x_2 + x_2')/b\delta] S^0(x_2, x_2', \mathbf{k}, \omega), \tag{3.13}$$

where

$$S^0(x_2, x_2', \mathbf{k}, \omega) = \int_{-\infty}^{\infty} dk_2 \exp[ik_2(x_2 - x_2')] u_*^3 \xi^4 \phi(k_+ \xi). \tag{3.14}$$

In Equation (3.14), ξ represents the geometric mean distance from the wall, $\xi = (x_2 x_2')^{1/2}$. k_+ is defined as:

$$k_+^2 = k_2^2 + \gamma^2 K_+^2, \tag{3.15}$$

and

$$K_+^2 = (\omega - U_c k_1)^2 / (hu_*)^2 + K^2, \tag{3.16}$$

where γ=constant and h is the velocity dispersion coefficient, which is considered a constant. The function $\phi(z)$ is approximately $(1+z)^{\lambda}$, where $3 < \lambda < 5$, although Chase discusses the behavior of the wall pressure spectrum for many limiting forms of λ. Examination of Equations (3.13)-(3.16) shows the dependence of the source spectrum on k_1, k_2, k_3 and ω.

Integration of the source spectrum, $S(x_2, x_2', \mathbf{k}, \omega)$, then yields the contribution of the turbulence-turbulence interaction to the wall pressure spectrum:

$$P_T(\mathbf{k},\omega) = \rho^2 K^2 \int_0^{\infty} x_2 \int_0^{\infty} x_2' e^{-K(x_2+x_2')} S(x_2, x_2', \mathbf{k}, \omega). \tag{3.17}$$

In a similar manner, integration of the source spectrum for the turbulence-mean shear interaction contribution yields the contribution of P_M to the point wall pressure spectrum.

The incompressible model of the wall pressure spectrum, as stated by Equation (39) in Chase's 1987 paper[15], with $\lambda = 3$, is:

$$P(\mathbf{k},\omega) = \frac{\rho^2 u_*^3}{\left[K_+^2 + (b\delta)^{-2}\right]^{5/2}} \left\{ C_T K^2 \left[\frac{K_+^2 + (b\delta)^{-2}}{K^2 + (b\delta)^{-2}} \right] + C_M k_1^2 \right\}, \tag{3.18}$$

where C_M and C_T are once again constants that must be determined by experimental data. The compressible model for the wavevector frequency spectrum is given by Chase

Equation (40) as:

$$P(\mathbf{k},\omega) = \frac{\rho^2 u_*^3}{\left[K_+^2 + (b\delta)^{-2}\right]^{5/2}} \left\{ \left[c_2 \left(\frac{|K_c|}{K} \right)^2 + c_3 \left(\frac{K}{|K_c|} \right)^2 \right. \right.$$
$$\left. \left. + 1 - c_2 - c_3 \right] C_T K^2 \left[\frac{K_+^2 + (b\delta)^{-2}}{K^2 + (b\delta)^{-2}} \right] + C_M \left(\frac{K}{|K_c|} \right)^2 k_1^2 \right\}, \tag{3.19}$$

where c_1, c_2 and c_3 are additional empirical constants. The compressibility enters into Equation (3.19) in the $(K/|K_c|)$ terms, where K_c is:

$$|K_c|^2 = \begin{cases} K^2 - \omega^2/c^2, & K > \omega/c \\ \omega^2/c^2 - K^2, & K < \omega/c \end{cases}. \tag{3.20}$$

Values for the empirical constants are once again established by comparisons to actual data. In this paper, Chase uses the data of Martin and Leehey[16] to determine the values of the empirical constants h, C_M, C_T, and b. In summary,

$$h = 3.0, \quad C_T = .0047, \quad C_M = 0.155, \quad b = 0.75. \tag{3.21}$$

In the compressible model, Chase assumes

$$c_2 = c_3 = 1/6, \tag{3.22}$$

although he admits there is no substantial experimental evidence to validate the values of c_2 and c_3. The value for these constants is arrived at by assuming an arbitrary ratio between the velocity source spectra.

As summarized by Chase, the differences between the 1980 model and the 1987 incompressible model are slight. When comparing the models with the empirical coefficients given in the respective papers, the contribution of P_T to the point pressure spectrum is lower in the 1987 model than in the 1980 model. In the high frequency limit of the point pressure spectrum, $P(\omega) = 1.06\rho^2 u_*^4 \omega^{-1}$, P_M is higher in the 1987 model than in the 1980 model. This increased contribution of P_M in the high frequency limit results in the mean shear term being predominant in the high frequency limit, where the turbulence-turbulence contribution was predominant in the 1980 model. Lastly, P_T is now considered to be the main contributor to the wall pressure spectrum in the subconvective range.

Chapter 4

EXPERIMENTAL MEASUREMENTS OF THE TURBULENT BOUNDARY LAYER WALL PRESSURE SPECTRUM

4.1 Methodology

Recent advances in the areas of signal processing and sensor technology have allowed for more accurate measurements of the wall pressure spectrum under a turbulent boundary layer. Many previous measurements have been contaminated by extraneous noise generated within the measurement facility. As will be discussed below, by utilizing additional signal processing techniques on the acquired data, it is possible to remove this contamination from the final result. The other major problem encountered in the measurement of the wall pressure spectrum is resolution of the high frequency components. The important length scale for the high frequency components is υ/u_*, which is on the order of the viscous sublayer thickness. Therefore, to accurately measure these components of the wall pressure spectrum, sensor sizes must be extremely small--of order υ/u_*.

In the following sections, measurements from three different experiments utilizing one or both of the above mentioned technologies will be presented. Three different fluids, glycerine, water, and air are represented in order to cover a broad range of experimental results.

4.2 Glycerine Experiment

An experiment in a glycerine tunnel was performed by Lauchle and Daniels[17]

utilizing both small transducers and advanced signal processing. The pressure transducers used allowed for d^+ in the range of $0.7 \leq d^+ \leq 1.5$, where d^+ is the transducer diameter in viscous wall units, du_*/υ. The small pressure transducers combined with the thick boundary layers generated in glycerine flow allowed better resolution of the high frequency components of the wall pressure fluctuations than had previously been achieved.

In this work, Lauchle and Daniels used an array of three circumferentially coplanar wall pressure transducers and radial accelerometers were mounted within the tunnel wall. The signals measured by the pressure transducers in the wall of the tunnel were considered to consist of four components: a turbulent boundary layer wall pressure component, a contribution from the acoustic background noise of the facility, a vibration induced pressure from the facility, and an electronic noise generated by the instrumentation. The electronic noise was measured to be more than 60 dB below the measured spectra so it was ignored. Given that the plane-wave cutoff frequency of the tunnel was calculated to be 4100 Hz, all acoustic noise components below 4100 Hz were considered to be circumferentially in phase. The contribution of the acoustic noise components to the measured spectrum below 4100 Hz could be negated by subtracting one pressure signal from another since the sensors were coplanar. It was postulated that if the vibration induced contamination was circumferentially coherent, these components could also be canceled by subtraction of one measured spectrum from another. By utilizing the coherent output power (COP) between an accelerometer difference signal and a pressure transducer difference signal, Lauchle and Daniels proved that the contribution of the vibration induced noise to the measured difference spectra was much lower than the turbulent wall pressure spectra contribution. This result was verified by another technique termed the cross-

difference technique. The cross-difference technique produces the result that the pressure-spectrum of the turbulent wall pressure is approximately equal to the cross-spectrum between two pressure transducer difference signals.

Figure 3 reproduces the results of Figure 11 in Lauchle and Daniels[17] for a Reynolds number based on pipe diameter of Re=10890. The spectra has been smoothed in the high frequency region to remove fluctuations in the measured level, which are a result of random errors in the measurement technique.

4.3 Water Experiment

Horne and Handler[18] performed an experiment in a water filled rectangular channel flow facility. The same type of pressure transducers as those used by Lauchle and Daniels[17] were utilized in this experiment. With water as the working fluid, these pressure transducers yielded a d^+ in the range $20 \leq d^+ \leq 40$. Pressure spectra were gathered and stored in a digital format for post-processing. The post-processing techniques utilized were able to remove the low frequency contamination from the measured pressure spectra, while the small transducers employed allowed for good resolution of the high frequency components.

Figure 4 shows Horne and Handler's fully corrected turbulent boundary layer spectrum for a tunnel Reynolds number of Rh=25000. The success of the signal processing techniques used by Horne and Handler were based on the validity of two assumptions: the correlation length of the noise contaminating the measurements was much larger than the correlation length of the turbulent boundary layer pressure fluctuations, and the turbulence was homogeneous in the spanwise direction. Using the first assumption,

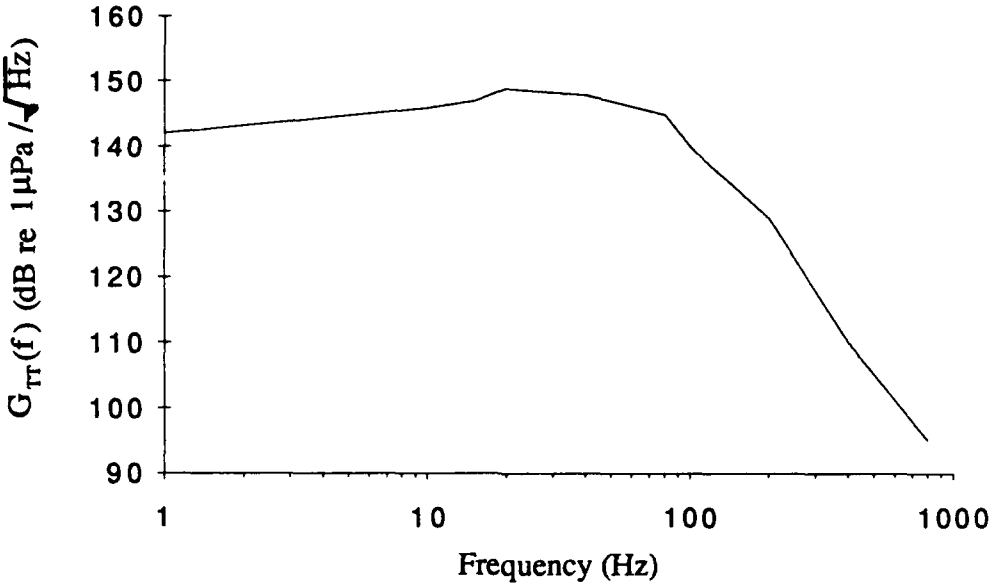

Figure 3 - Measured Wall Pressure Spectra for Glycerine Pipe Flow Facility at Re=10890

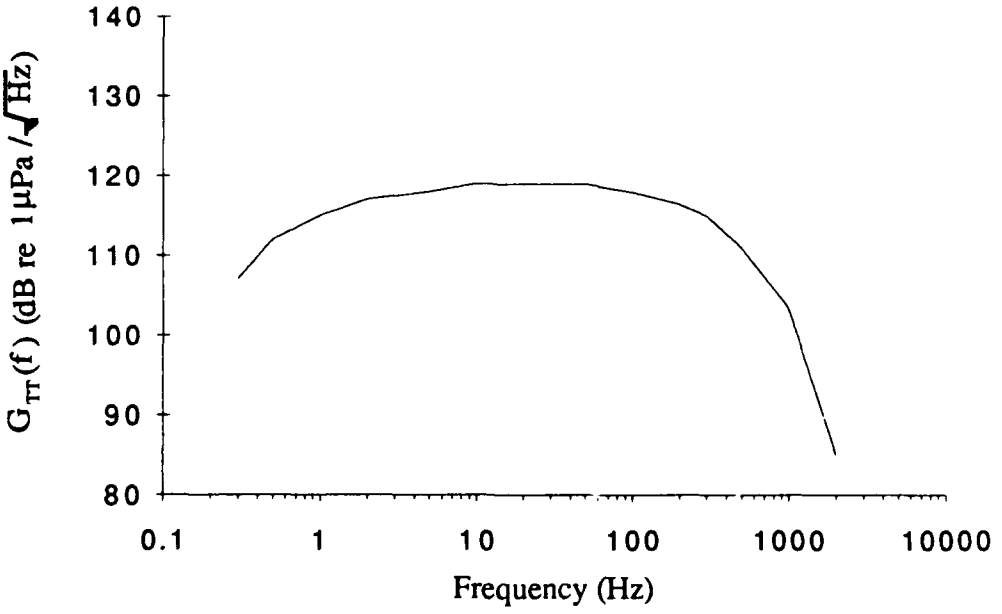

Figure 4 - Measured Wall Pressure Spectra in Rectangular Water Channel at Rh=25000

the pressure spectrum is corrected using a least mean square algorithm. The pressure spectrum was further corrected using a factor based upon the coherence between the two sensors.

4.4 Air Experiment

An experiment utilizing very small pressure transducers was performed by Schewe[19] in a wind tunnel. Schewe developed an electrostatic transducer of the Sell type to achieve d^+ values in the range of $19 \leq d^+ \leq 333$. The smallest pressure sensor utilized by Schewe had an active diameter of 1 millimeter which corresponds to $d^+=19$. Figure 5 shows the turbulent boundary layer pressure spectrum measured by Schewe using his smallest pressure transducer at a free-stream velocity of $U_\infty = 6.3$ m / s. This velocity corresponds to a Reynolds number of $Re_\theta = 1400$ based on a momentum thickness of $\theta = 3.3$ mm.

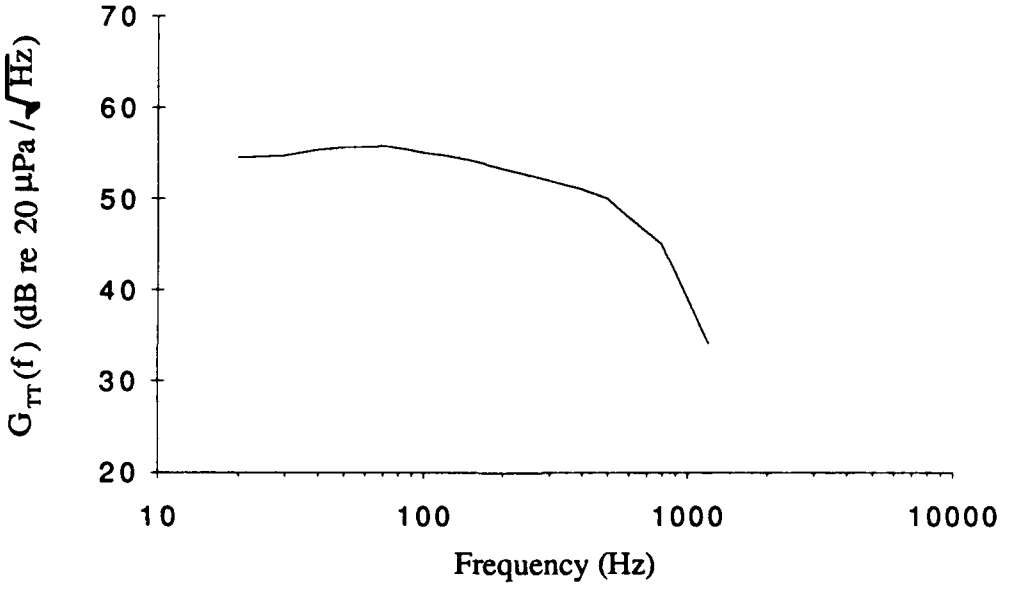

Figure 5 - Measured Wall Pressure Spectra for Wind Tunnel at Re_θ=1400

Chapter 5

NUMERICAL INTEGRATION OF THE WAVEVECTOR-FREQUENCY SPECTRUM

5.1 Two-Dimensional Simpson's 1/3 Method

Prediction of the turbulent boundary layer pressure fluctuations were obtained by numerically integrating Equation (3.1). The integration of Equation (3.1) is performed using a two dimensional Simpson's 1/3 rule.[20] The integration is carried out by shifting Simpson's 1/3 rule for one dimension into two dimensions. The general form of the Simpson's 1/3 rule, which is used to integrate a function f(x,y), is:

$$I = \int_{x_{i-1}}^{x_{i+1}} \int_{y_{i-1}}^{y_{i+1}} f(x,y)dxdy = \frac{k}{3}\left[\frac{h}{3}(f_{i+1,j+1} + 4f_{i,j+1} + f_{i-1,j+1})\right.$$
$$\left. +4\frac{h}{3}(f_{i+1,j} + 4f_{i,j} + f_{i-1,j}) + \frac{h}{3}(f_{i+1,j-1} + 4f_{i,j-1} + f_{i-1,j-1})\right]. \qquad (5.1)$$

To evaluate Equation (3.1), the integration was carried out in the k_1 and k_3 directions. At each point in wavenumber space where the integration is performed, a rectangle consisting of nine locations is defined. This rectangle has dimensions of twice the step size in the k_1-direction by twice the step size in the k_3-direction. The function f(x,y) is the wavenumber-frequency spectra proposed by Chase in both his 1980 and 1987 papers. For the 1980 model equation, Equations (3.9) and (3.10) are used in Equation (5.1) for f(x,y). For the incompressible model in Chase's 1987 paper, Equation (3.18) is integrated; and for Chase's compressible model, Equation (3.19) is integrated.

5.2 General Parameters

Determination of the general parameters to be used for the integration in all three cases; air, water and glycerine, is the next step in carrying out the integration. Based upon an examination of the wavenumber dependence of the turbulent wall pressure spectrum, and from previous experience in evaluating Equation (3.1)[21], values for the upper and lower limits of integration were established. For all cases, in both the k_1 and the k_3 directions, the double integral is evaluated at 80 locations in the range $-10k_c$ to $10k_c$. For each case, the spectral level for 30 frequency points between the lowest and highest frequencies of interest are calculated. Due to the finite limits necessary to carry out the numerical integration the results represent a lower bound on the magnitude of the wall pressure spectra. The frequency range of interest depends upon the data available for each fluid. Depending on the author, various frequency dependent values of the convective velocity have been established. Most of these models show only a weak dependence on frequency, so a constant value of convective velocity was used for the calculations. For this paper, as was used by Chase in his 1987 paper, the value of the convective velocity is taken to be $.65U_\infty$. Based on calculations for the wall pressure spectrum with convective velocities ranging from $.6U_\infty$ to $.8U_\infty$, it is noted that the effect of choice for the convective velocity was minimal on the results of the calculations.

One important point to note is that the experiment in water was performed in a rectangular channel facility and the glycerine experiment was performed in a pipe flow facility. For both of these cases, the turbulent boundary layer was not a free boundary layer as was modeled by Chase in his two papers. The boundary layer thickness for the bounded cases were, therefore, considered to be the half-height of the corresponding facility.[2]

The friction velocity, and when necessary, the wall shear stress are calculated based on formulas given by White.[2] The wall shear stress is given by Equation (2.3) and the friction velocity is given by Equation (2.7). As can be seen by examination of these equations, the most important factor for calculating these parameters is the Reynolds number, which was given in Chapter 4 for all three cases of interest.

5.2.1 Constants for Chase's 1980 Model

The empirical constants used in the wavevector-frequency spectra were established based on the work of Chase[12] and Lauchle[10]. The values for b_M and b_T are those given by Chase; and the values for h_M, h_T, C_M, and C_T are those given by Lauchle. The constants used for the integration of Chase's 1980 model are:

$$\begin{aligned} &b_M = 0.756 \quad b_T = 0.378 \quad h_M = 20.0 \\ &h_T = 20.0 \quad C_M = 0.05 \quad C_T = .004\ . \end{aligned} \tag{5.2}$$

5.2.2 Constants for Chase's 1987 Models

To establish the empirical constants for his compressible and incompressible models, Chase used the work of Martin and Leehey[16]. The six constants used in the incompressible and compressible model are:

$$\begin{aligned} &h = 3.0 \quad b = 0.75 \quad C_T = 0.0047 \\ &C_M = 0.1553 \quad c_1 = 0.1667 \quad c_2 = 0.1667\ , \end{aligned} \tag{5.3}$$

where c_2 and c_3 are only used for the compressible model.

5.3 Flow Parameters for Glycerine Experiment

The glycerine experiment of Lauchle and Daniels[17] was performed in a pipe flow facility for a range of Reynolds numbers. The experimental facility is designed to change the Reynolds number by varying the temperature of the working fluid as opposed to varying the flow velocity. The flow velocity at the centerline of the tunnel is stated as $6.8\ m/s \le U_{av} \le 7.5\ m/s$. The mean value of this stated range was chosen for the free-stream velocity. Fluid properties at 35° C were used for the calculations, boundary layer thickness was assumed to be the radius of the tunnel, and the sensor diameter was given as 0.5 mm. Based on this information, the following values were used to calculate spectral levels for the glycerine tunnel experiment:

$$\begin{aligned} &Re = 10890 \quad \rho = 1238\ kg/m^3 \quad U_{av} = 7.15\ m/s \quad R = 0.25\ mm \\ &\delta = a = 0.14\ m \quad U_c = 4.648\ m/s \quad u_* = 0.441\ m/s \quad \tau_\omega = 240.93\ Pa \\ &\upsilon = 1.72 \times 10^{-4}\ m^2/s \quad c = 1980\ m/s \end{aligned} \tag{5.4}$$

where the values of convection velocity, wall shear stress, and friction velocity were calculated by the program. Since this flow is in a pipe, the equation used for calculation of wall shear stress is different from the one used for a flat plate[5]:

$$\tau_\omega = 0.0325 \rho U_{av}^{7/4} \upsilon^{1/4} a^{-1/4}\ , \tag{5.5}$$

where a is the pipe radius and U_{av} is the average pipe flow velocity. The spectral calculations were performed over the frequency range of 1-1000 Hz. Based on these parameters, the solid line of Figure A1 shows $P(k_1,0,\omega)$ computed from the 1987 compressible model, for a frequency of f=100 Hz.

5.4 Flow Parameters for Water Experiment

The experiment with water was performed in a rectangular channel flow facility. Given the channel Reynolds number, channel dimensions, and that the working fluid was water at approximately 20° C; the following parameters were used for the calculations:

$$\begin{aligned} &Rh = 25000 \quad \rho = 998\ kg/m^3 \quad U_{av} = 1.7\ m/s \quad R = 0.25\ mm \\ &\delta = a = 0.0125\ m \quad U_c = 1.105\ m/s \quad u_* = 0.089\ m/s \\ &\tau_\omega = 7.953 Pa \quad \upsilon = 1.005 \times 10^{-6}\ m^2/s \quad c = 1481\ m/s\,. \end{aligned} \tag{5.6}$$

Once again, the values for convection velocity, wall shear stress, and friction velocity were calculated by the program. Wall shear stress was calculated using equation (5.5), and spectral calculations were performed over the frequency range 0.2-2000 Hz. Based on these parameters, the solid line of Figure A2 shows $P(k_1,0,\omega)$ computed from the 1987 compressible model, for a frequency of f=100 Hz.

5.5 Flow Parameters for Air Experiment

The experiment by Schewe[19] was performed in a wind tunnel. For this experiment, all the necessary flow parameters were given. The only parameter calculated by the program was the convective velocity. The parameters used for the calculation of the spectral levels for the experiment in the wind tunnel were:

$$\begin{aligned} &Re_\theta = 1400 \quad \rho = 1.20\ kg/m^3 \quad U = 6.3\ m/s \quad R = 0.5\ mm \quad \delta = 30\ mm \\ &U_c = 4.095\ m/s \quad u_* = .273\ m/s \quad \tau_\omega = .09\ Pa \quad c = 343\ m/s\,. \end{aligned} \tag{5.7}$$

Spectral levels were calculated for the frequency range of 20-2000 Hz. Based on these parameters, the solid line of Figure A3 shows $P(k_1,0,\omega)$ computed form the 1987 compressible model, for a frequency of f=100 Hz. Due to the slower speed of sound in air relative to the other fluids, the acoustic wavenumber is present on Figure A3. The acoustic wavenumber can be seen to effect $P(k_1,0,\omega)$ at $k_1 / (\omega / U_c) \approx .012$.

Chapter 6

RESULTS

6.1 Constants Given By Chase

In this section, a comparison of the three models proposed by Chase in his 1980 and 1987 papers will be presented. Spectral levels were first calculated using all three of Chase's models with the constants specified in Chapter 5. This first comparison will allow one to assess the differences among the various models proposed by Chase. Figure 6 shows the spectral levels calculated for the glycerine experiment for all three models; Chase's 1980 model, the 1987 incompressible model, and the 1987 compressible model. Notice that the 1987 compressible model and the 1987 incompressible model result in the same predicted spectral levels for the given constants. The 1980 and 1987 models predict the same spectral shape but with different amplitudes.

Figure 7 shows the spectral predictions for the water flow experiment. The low frequency region of Figure 7 illustrates one of the main differences between Chase's 1980 and 1987 models. As stated in Section 3.2.2, the assumption that $P(\mathbf{k},\omega)$ tends to zero as K^2 was relaxed in the 1987 models. This is evident by the change in slope between the two models in the low frequency region.

Figure 8 shows the results predicted by the 1980 and 1987 models for the flow parameters given by Schewe in his wind tunnel experiment. The results in Figure 8 show similar trends as those in Figure 6 for the glycerine experiment. The low frequency divergence between the two models can be seen to be starting at the lowest data point, 20 Hz. If the calculations were carried out to lower frequencies, the results would show the

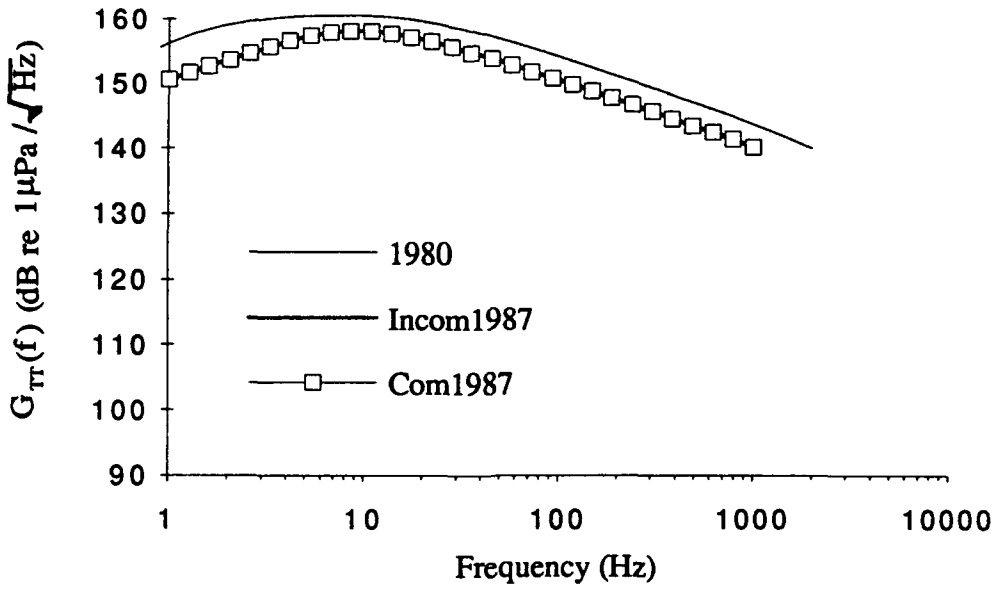

Figure 6 - Comparison of Chase Models for Glycerine Flow Parameters

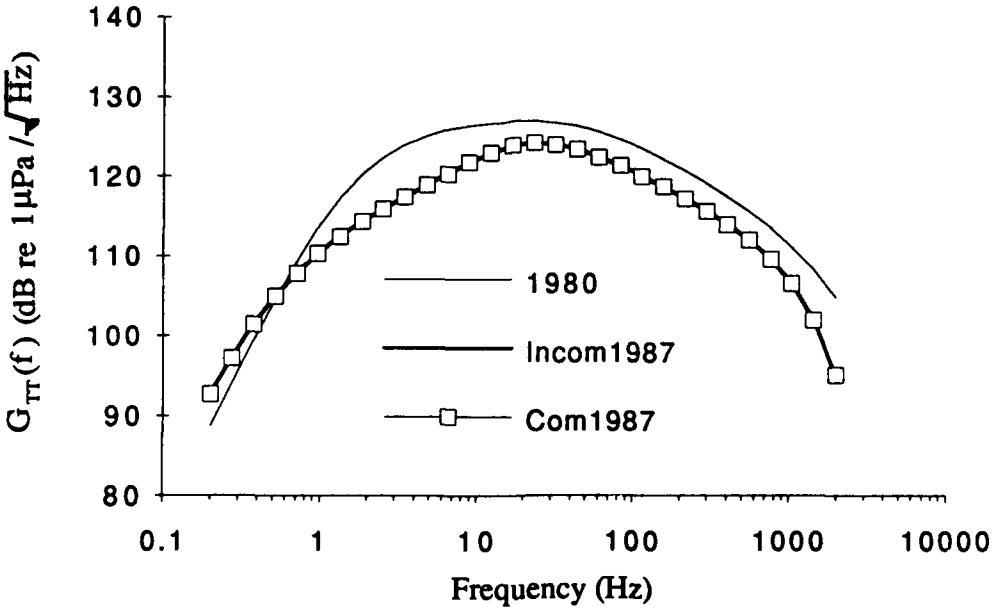

Figure 7 - Comparison of Chase Models for Water Flow Parameters

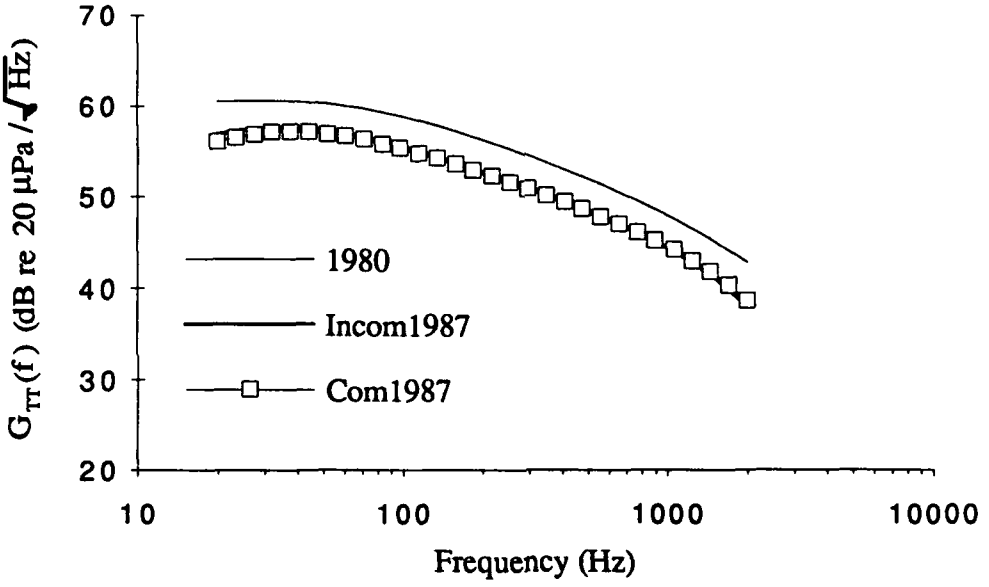

Figure 8 - Comparison of Chase Models for Air Flow Parameters

same trend as the low frequency data in Figure 7.

6.1.1 Comparison to Experimental Results

A comparison of the spectral levels calculated with the given constants versus the experimental results are presented in this section. Since the calculated results obtained for the incompressible and compressible 1987 models were the same, only the compressible model results will be displayed. Figure 9 shows a comparison between calculated values and experimental values for the glycerine experiment. A number of discrepancies between predicted and measured levels can be noted. The spectral levels predicted by all three models were considerably higher than those measured. The predicted peak level occurs at around 10 Hz, while the measured peak level occurs at about 20 Hz. The measured levels decrease rapidly after the peak value while the predicted values decrease at a much slower rate. This marked difference in spectral level above 100 Hz may be a result of the fact that Chase's models do not take into account the viscous domain of the turbulent boundary layer. Based on the work of Farabee and Casarella[22], the source of the high frequency portion of the wall pressure spectrum is proposed as the overlap region of the boundary layer. The small scale velocity fluctuations in this region are affected by the viscosity of the fluid. By neglecting the effect of viscosity, Chase may be over predicting the small scale, high frequency, velocity fluctuations. Another issue to be considered for these discrepancies is the use of an external flow prediction method for an internal flow.

A comparison between measured and predicted spectral levels for the water tunnel experiment of Horne and Handler[18] is shown in Figure 10. The agreement between measured and predicted values is much better for this experiment. In the higher frequency range, above about 100 Hz, Chase's models predict the rate of decrease of the spectral

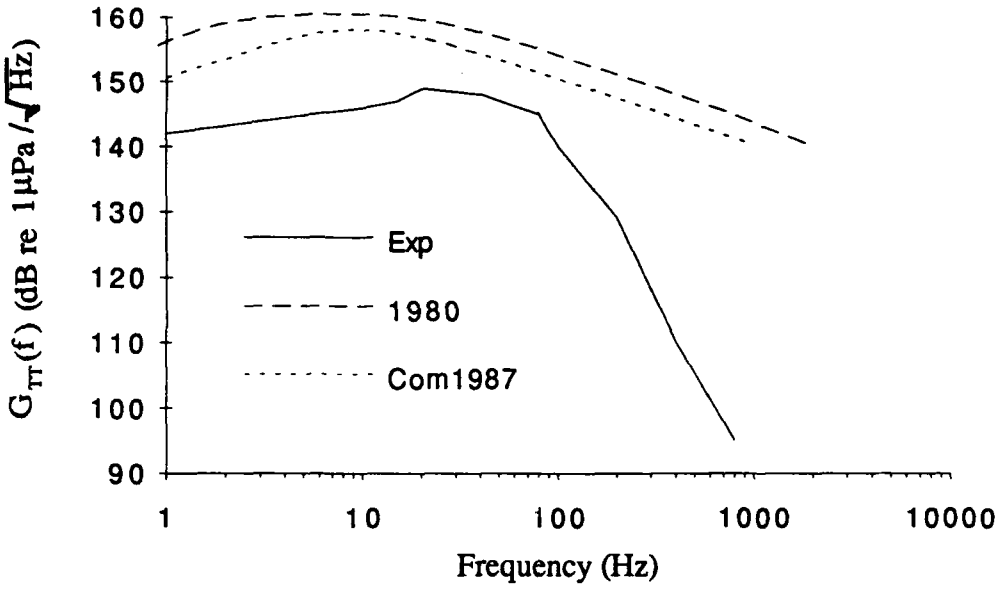

Figure 9 - Calculated vs. Measured Values for Glycerine Experiment

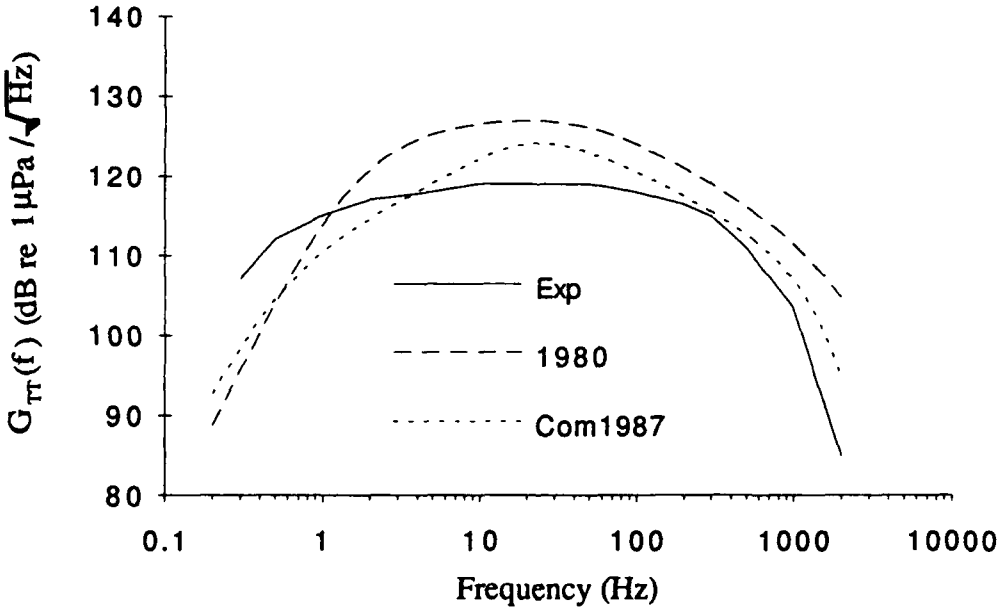

Figure 10 - Calculated vs. Measured Values for Water Experiment

levels much more accurately for the water experiment than for the glycerine experiment. By comparing Figures 9 and 10, one can see that above 100 Hz the negative slope of the measured pressure spectrum is much greater for glycerine than water. In the low frequency region, below about 5 Hz, all three models decrease more rapidly than the measured levels. As noted above, the 1987 models decrease less rapidly than the 1980 model in the low frequency region, although the results are still too low.

Figure 11 shows the comparison between measured and calculated spectral levels for the wind tunnel experiment of Schewe[19]. The predictions of the 1987 models show relatively good agreement with the actual measured levels. Once again, the high frequency region is the area where the agreement between measured and predicted levels is the poorest. In this case, the predicted levels agree well with the experimental results up to about 900 Hz.

In general, the agreement between measured and predicted levels for the air and water data is good. The predictions for the glycerine experiment show poor agreement with experimental results. The predictions with the 1987 models, both incompressible and compressible, show better agreement with experimental results than the predictions using the 1980 model. In all cases, as one progresses to higher frequencies, Chase's models tend to over predict the measured sound pressure levels. In the following section, an attempt will be made to obtain a better fit to the experimental data by varying the six empirical constants utilized by Chase in his 1987 compressible model.

6.2 Empirical Constants

In order to obtain a better agreement between the experimental and calculated results,

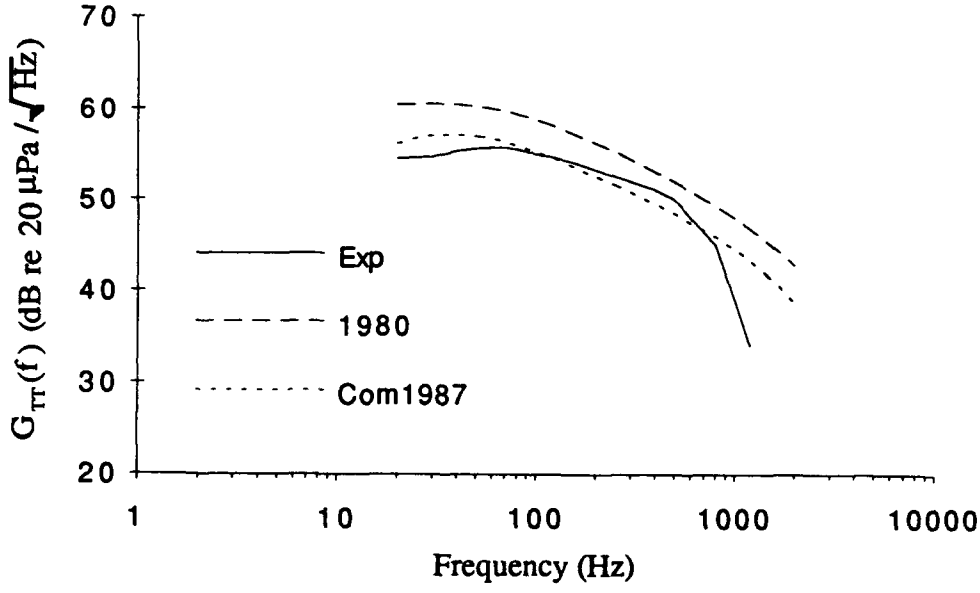

Figure 11 - Calculated vs. Measured Values for Air Experiment

the six parameter values given by Chase for his 1987 incompressible model were systematically varied. The first step was to vary each parameter individually to quantify the effect each parameter has on the calculated wall pressure spectrum. As an example, Figure 12 is a comparison of the spectral levels calculated for the air experiment with the values given by Chase versus the spectral levels calculated when C_T is reduced by a factor of 3. All other constants remained the same for this calculation. One can see that reducing the value of C_T by a factor of 3 had very little effect on the calculated spectral levels. Figure 13 shows the result of lowering the value of C_M by a factor of 3 while keeping the other parameters constant. As shown by Figure 13, reducing the value of C_M reduced the overall levels by about 5 dB. Reducing C_M by the same factor as C_T had a much greater impact on the predicted levels. This is to be expected since the contribution to the turbulent boundary layer wall pressure by the mean shear-turbulence interaction term is significantly larger than the contribution from the turbulence-turbulence interaction term. Another important feature of both Figures 12 and 13 is that, although the magnitude of the predicted levels was changed, the shapes of the spectra remained identical. Figure 14 compares the results for the given constants to the values predicted by the model when b is reduced by a factor of 3. The effect of b, the scale coefficient, on the low frequency predicted levels is considerable. Below 300 Hz, the lower value of b causes divergence between the spectral levels predicted with the original constants. Above about 300 Hz, the new set of data matches the original predicted levels. Finally, Figure 15 shows calculations when h is lowered by a factor of 3. The effect of the velocity dispersion coefficient, h, is similar to that of C_M. The level of the entire spectrum is reduced by about 5 dB, but the slope of the predicted curve remains the same. Varying the parameters c_1 and c_2 had an extremely small effect on the calculated wall pressure spectrum.

Figure A1 shows the results of varying the empirical constants C_M, h, and b on

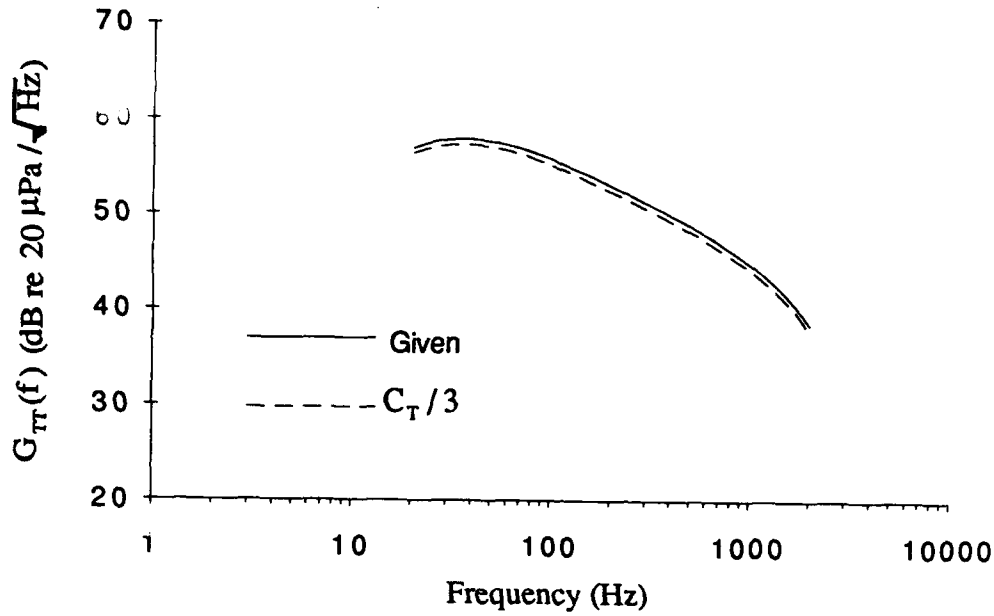

Figure 12 - Calculated Spectral Levels for Given Constants vs. $C_T / 3$ for Air Experiment

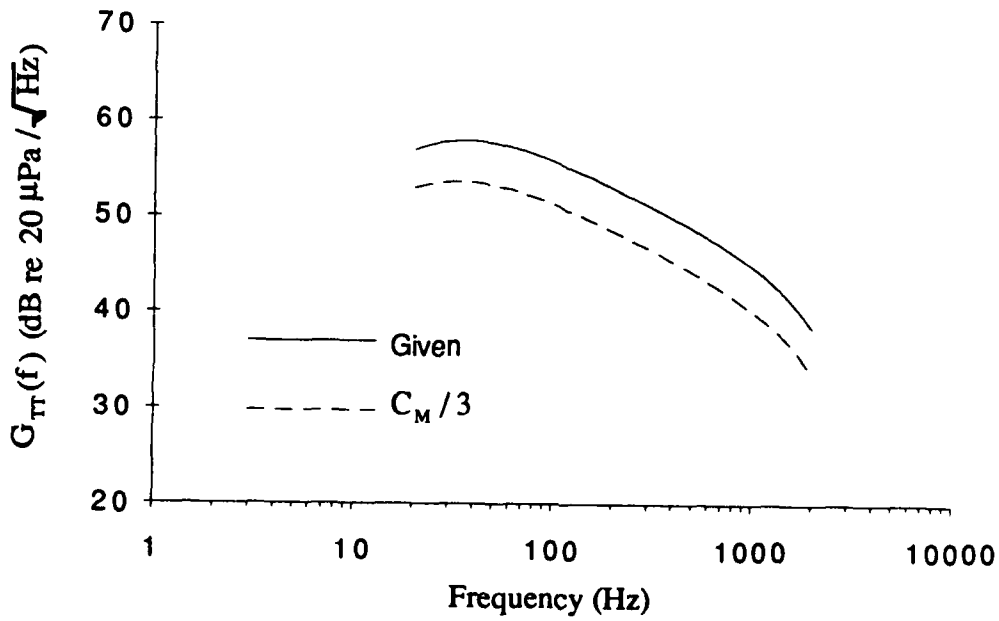

Figure 13 - Calculated Spectral Levels for Given Constants vs. $C_M / 3$ for Air Experiment

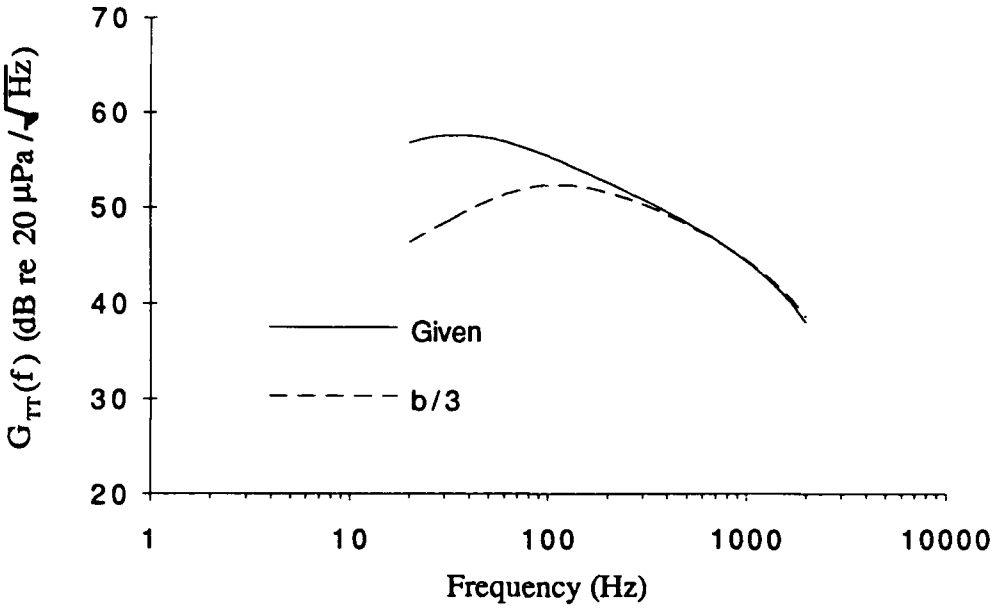

Figure 14 - Calculated Spectral Levels for Given Constants vs. b/3 for Air Experiment

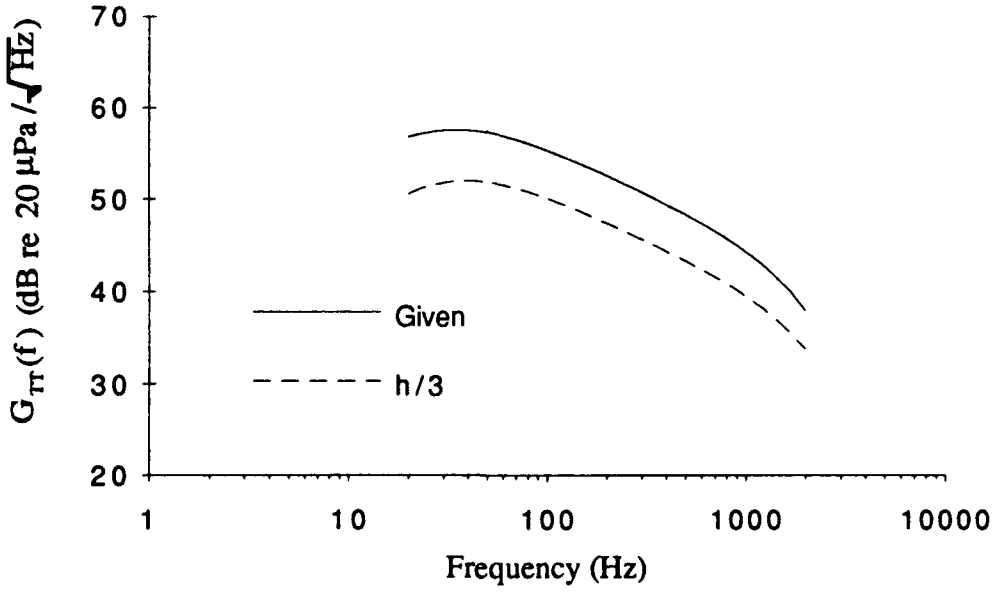

Figure 15 - Calculated Spectral Levels for Given Constants vs. h/3 for Air Experiment

$P(k_1,0,\omega)$ for the glycerine experiment flow parameters at a frequency of 100 Hz. Note the overall level of $P(k_1,0,\omega)$ for the original constants vs. the best fit constants. Figure A2 shows the results of varying the empirical constants C_M, h, and b on $P(k_1,0,\omega)$ for the water experiment at a frequency of 100 Hz. For the water experiment, the best fit result for $P(k_1,0,\omega)$ is much closer to the original result than is the case for the glycerine experiment. Figure A3 shows the results of varying the empirical constants C_M, h, and b on $P(k_1,0,\omega)$ for the air experiment at a frequency of 100 Hz.

Inspection of Figures 12-15 shows that the only parameter that changes the general shape of the spectrum is b. The effect of the scale coefficient, b, is most noticeable in the low frequency region of the wall pressure spectrum. None of the parameters have any impact on the slope of the high frequency end of the spectrum. This fact will limit the effectiveness of fitting the experimental data by varying the empirical constants.

6.2.1 Empirical Fit to Experimental Data

Using the information gained by varying the constants individually, an empirical best fit to the experimental data was obtained by varying combinations of the empirical parameters. The combinations used are not necessarily unique. In general, the scale coefficient, b, was used to fit the slope of the low frequency calculated data to the experimental data. The overall level was adjusted using combinations of h and C_M. Due to the relatively minor impact of C_T on the calculated pressure spectrum, its value was unchanged.

Figure 16 is a comparison of the experimental data for the air experiment with the best fit obtained by varying Chase's empirical parameters. The final parameter values used in

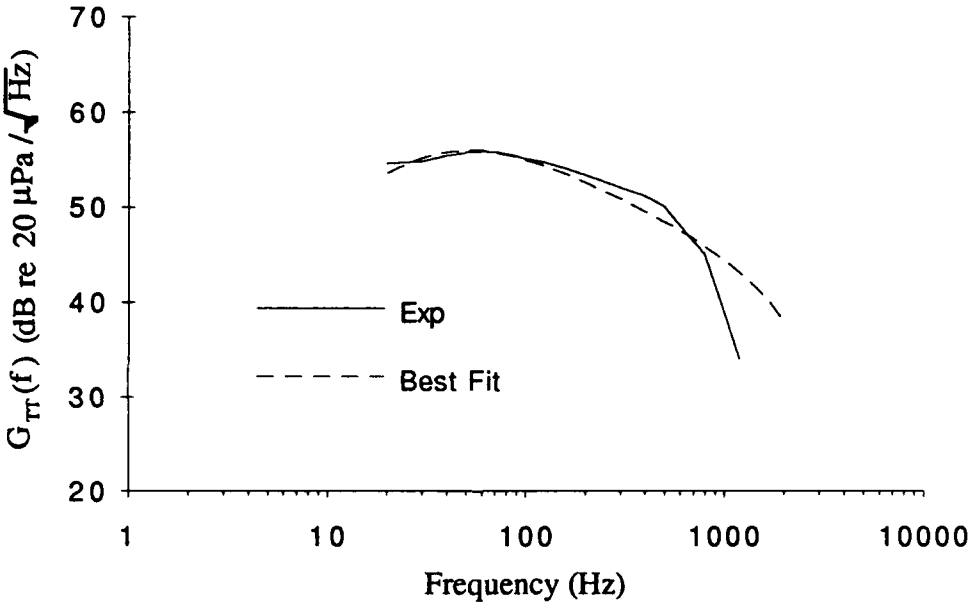

Figure 16 - Experimental Data for Air Experiment vs. Best Fit Data with 1987 Compressible Model

the 1987 compressible model are:

$$h = 3.0 \quad b = 0.5 \quad C_T = 0.0047$$
$$C_M = 0.2330 \quad c_1 = 0.1667 \quad c_2 = 0.1667 . \tag{6.1}$$

Comparison of these values with Equations (5.3), the original value of the constants, illustrates the changes made. Although b was altered by a significant amount, the remainder of the values were changed very little. Since the original values of constants used by Chase were determined by comparison to wind tunnel data, this is not unexpected. The low frequency portion of the experimental curve was fit by reducing the value of b. The overall levels were adjusted using a slightly higher value of C_M. The calculated spectral levels agree well with the experimental data up to about 1000 Hz. The measured peak level is at about 50 Hz and the calculated peak level, with the above values of experimental parameters, now coincides with this peak. Above 1000 Hz, the model still over predicts the sound pressure levels. As mentioned above, none of the experimental parameters can affect solely the high frequency end of predicted pressure spectrum. With the Chase's present model of the turbulent boundary layer, it is not possible to match the low frequency and high frequency portions of Schewe's measured pressure spectrum.

Figure 17 is a comparison of the Horne and Handler experimental data for the water experiment with the best fit obtained by a new set of empirical parameters. The final parameter values used in the 1987 compressible model are:

$$h = 3.0 \quad b = 1.40 \quad C_T = 0.0047$$
$$C_M = 0.0777 \quad c_1 = 0.1667 \quad c_2 = 0.1667 . \tag{6.2}$$

Once again, the low frequency portion of the spectrum was fit using the scale coefficient b.

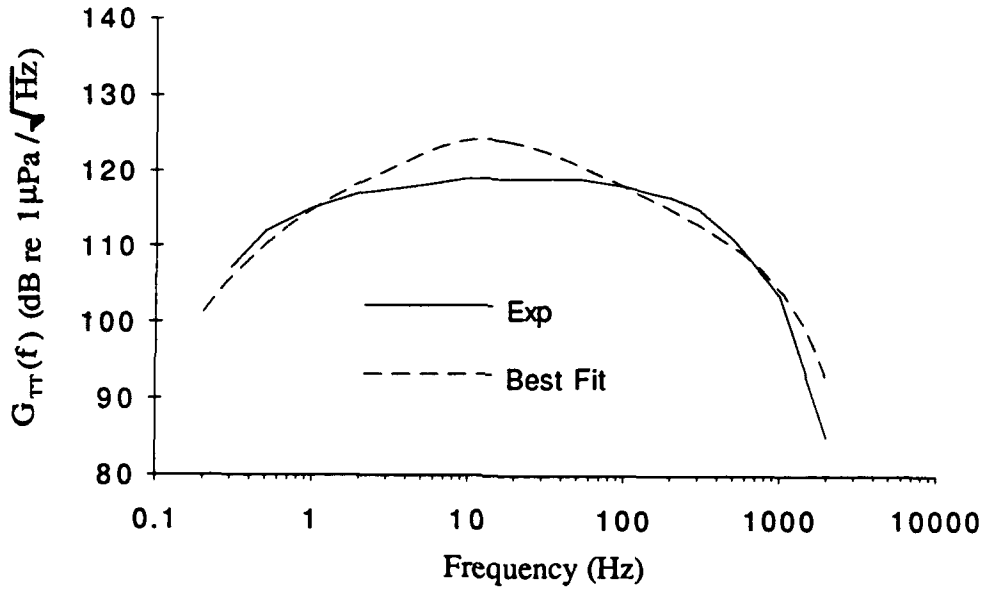

Figure 17 - Experimental Data for Water Experiment vs. Best Fit Data with 1987 Compressible Model

After the low frequency end of the spectrum was fit, the overall level was adjusted using C_M. There is good agreement between the calculated and measured values for the water experiment in the low and high frequency regions. The peak predicted spectral level of the wall pressure spectrum was at about 20 Hz. The measured wall pressure spectrum shows a peak in the same region, although lower in level by about 9 dB. Above 1000 Hz, the measured and predicted levels begin to diverge, although not as noticeably as in the case of the air data.

Figure 18 is a comparison of the experimental data for the glycerine experiment of Lauchle and Daniels with the best fit obtained by varying Chase's empirical parameters. The final parameter values used in the 1987 compressible model are:

$$\begin{aligned} &h = 1.0 \quad b = 0.4 \quad C_T = 0.0047 \\ &C_M = 0.10 \quad c_1 = 0.1667 \quad c_2 = 0.1667 \,. \end{aligned} \tag{6.3}$$

Above 100 Hz, there are still large discrepancies between measured and predicted spectral levels. Glycerine, having the highest viscosity of the three fluids under consideration, exhibits the poorest high frequency agreement between measured and predicted spectral levels. The measured peak spectral level is in the 20-30 Hz region. The predicted peak spectral level now corresponds with the measured peak. At frequencies below about 5 Hz, the predicted spectrum tends towards zero much more rapidly than the measured curve.

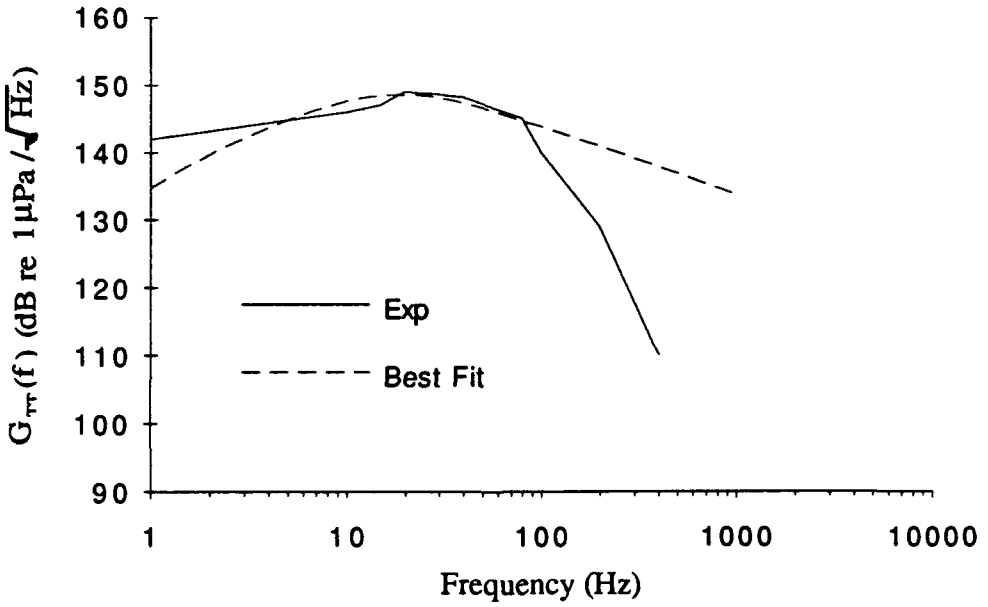

Figure 18 - Experimental Data for Glycerine Experiment vs. Best Fit Data with 1987 Compressible Model

Chapter 7
CONCLUSIONS

7.1 Justification for New Empirical Constants

In order to obtain a better fit to the measured wall pressure spectra presented in this paper, the values of the empirical constants used by Chase in his 1987 compressible model were varied. Having determined the values which are most suitable for the experiments considered, the reasons why these changes were necessary must be explored. In essence, two parameter values were varied. The first was the scale coefficient b, which changed the low frequency portion of the calculated wall pressure spectra. The second was the value of the product $C_M h$, which changed the overall level of the spectrum.

For the experiment performed in air, significant change in b was required. Chase[15] states that the scale coefficient, b, is used to cut off contributions to the wall pressure spectrum at wavenumbers less than the reciprocal of the outer scale, i.e. the boundary layer thickness. As noted, the scale coefficient affects the low frequency portion of the predicted wall pressure spectrum. Better agreement with Schewe's data was obtained by lowering the value of b from the value first postulated by Chase. This is to be expected because Chase[12] notes variability from experiment to experiment for the low frequency portion of the wall pressure spectrum. Based on this fact, it is not unexpected that the value of b needed to fit Schewe's data was different than the value of b needed to fit Martin and Leehey's data. The work done by Schewe was performed in a quiet wind tunnel designed for flow noise measurements. With this facility, it is possible that Schewe was able to obtain a better measurement of the low frequency portion of the wall pressure spectrum.

The value of the product $C_M h$ was increased by 1.5 times over the value used by Chase in his 1987 paper. This change, in part, was necessitated by the effect that decreasing b had on the mid frequency portion of the predicted spectrum. The result of this increase in $C_M h$ on the prediction is not significant, about 2-3 dB.

For the experiment performed in the water tunnel, so that the low frequency portions of the measured and predicted spectra would agree, the scale coefficient had to be increased by almost 3 times the original value. There are a number of possible causes for the need for this large increase. The experiment was performed in a rectangular flow facility so the boundary layer was bounded, not free. As was discussed by Farabee and Casarella[22], the physical characteristics of channel and flat plate boundary layer flows are different, especially in the outer regions, which generate the low frequency components of the wall pressure spectrum. A second possible cause is the presence of low frequency noise contamination in the measured signal. Although a significant decrease in measured levels was obtained by post-processing the acquired data to remove background noise, it is still possible some contamination remains. As was the case for the air experiment, the value of $C_M h$ was adjusted, lowered in this case, to compensate for the increase in b. The decrease in value of the product $C_M h$ did not totally compensate for the increase in h, which resulted in the mid frequencies of the predicted spectrum being slightly higher than originally predicted.

For the glycerine experiment, the greatest changes in the values of the constants were required. The product $C_M h$ was lowered by almost a factor of 5 to bring the overall levels into closer agreement with the measured levels. The velocity dispersion coefficient, h, is an empirical constant which is used to scale the friction velocity u_*. Comparison of the friction velocity for the air and glycerine shows that u_* is twice as large for the glycerine

experiment. The large value of u_*, coupled with the level of the coefficient h established for wind tunnel data resulted in spectral levels which were too high. The value of the coefficient used to scale the mean shear-turbulence interaction term, C_M, was also established by Chase based on wind tunnel data. Even if h was lowered by a factor of 2 to account for a higher friction velocity, C_M would still be too high. The value of b was lowered in an attempt to fit the low frequency portion of the spectrum. Below 5 Hz, the predicted levels are still decreasing more rapidly than measured. The same possible explanations apply to this data as for the water tunnel data

It is interesting to note the similarity between the results for the glycerine and water experiments. In both cases, the measured low frequency spectral levels decrease at a much slower rate than is predicted by Chase models. Both experiments utilized techniques to remove low frequency contamination from the acquired data. This leads to the conclusion that the similar results for the glycerine and water experiments may be the result of these being bounded shear flows rather than free boundary layers.

7.2 General Conclusions

This paper has attempted to evaluate the suitability of applying Chase's comprehensive wavevector frequency spectrum models[12,15] to the prediction of measured turbulent boundary layer wall pressure spectra. In the course of this investigation, a number of conclusions have been reached:

-The 1987 compressible and incompressible models predict spectral levels that are closer to measured levels than does the 1980 model.

-In the 1987 models, the functional dependence of the low frequency region of the

wavevector frequency spectrum was relaxed from the K^2 dependence of the 1980 model. Changing the low frequency dependence of the 1987 models resulted in better estimates of the very low frequency regions of the wall pressure spectrum, as can be noted in comparison with data from the water tunnel. Although better, the models still tend to over predict the rate of decrease of the spectral levels in the low frequency region of the spectrum for the water and glycerine experiments.

-In his 1980 paper, Chase states that the effect of viscosity on the convective ridge of the wavevector-frequency spectrum will be small provided $\omega\upsilon/u_*^2 \leq 2$, and that the effect of viscosity on the low wavenumber domain will be small if $\omega\upsilon/u_*^2 \leq 1/2$. For the glycerine experiment, this corresponds to viscous effects becoming important in the low wavenumber domain for frequencies above 90 Hz, and for the convective domain at frequencies above 360 Hz. The final results for the glycerine experiment, Figure 18, shows the calculated values deviating from the measured values at frequencies above about 90 Hz. For the water experiment, the above criteria correspond to frequencies of f=627 Hz and f=2508 Hz, for the low wavenumber and convective regions respectively. For the air experiment, viscous effects become important at frequencies of f=393 Hz and f=1571 Hz, for the low wavenumber and convective regions respectively.

-In all cases, the models over predict the measured spectral levels in the high frequency region. The cause of this appears to be that the models do not take into account the viscous domain of the turbulent boundary layer. Within the viscous sublayer, small scale, high frequency velocity fluctuations are reduced in magnitude. The best example of this is the comparison of the glycerine tunnel data to predicted levels.

-The models, in their present form, appear to be most suitable for predicting spectral levels of free boundary layers in nearly inviscid fluids. This is expected since Chase arrived at his models with such assumptions.

-A comparison of calculated wall pressure spectra, with the new empirical values

arrived at here, to a recent measurement of wall pressure spectral levels for a free boundary layer in water would be useful. This comparison should answer the questions concerning the rate of decrease of the low frequency spectral levels of the measured wall pressure spectra for the water and glycerine experiments.

- Comparisons of calculated wall pressure spectra, with the new empirical values, to a variety of recent air tunnel measurements would allow one to evaluate the applicability of the new constants to a range of flow conditions.

-Future work in modeling the wall pressure spectrum of the turbulent boundary with Chase's models should include an attempt to account for the effects of the viscous region of the turbulent boundary layer. Once a high frequency dependent term is included in Chase's wavevector-frequency spectrum model, a better match to the entire measured frequency spectrum may be obtained.

REFERENCES

[1] Willmarth, W.W., "Pressure Fluctuations Beneath Turbulent Boundary Layers," Annual Review of Fluid Mechanics, **7** (1975) 13-37.

[2]White, F.M., *Fluid Mechanics*, McGraw Hill, Inc., 1979

[3]Schlichting, H., *Boundary Layer Theory* , 7th Edition, McGraw Hill Inc., 1979.

[4]Tennekes, H., and Lumley, J.L. *A First Course in Turbulence*, The MIT Press, 1972.

[5]White, F.M., *Viscous Fluid Flow*, McGraw Hill, Inc., 1974

[6]Kraichnan, R.H., "Pressure Fluctuations in Turbulent Flow over a Flat Plate," *J. Acoust. Soc. Amer.*, **28** (1956) 378-390

[7]Blake, W.K., *Aero-Hydroacoustics for Ships*, David W. Taylor Naval Ship Research and Development Center, Report No. DTNSRDC-84/010 (1984)

[8]Farabee, T.M., "An Experimental Investigation of Wall Pressure Fluctuations Beneath Non-Equilibrium Turbulent Flows," *David W. Taylor Naval Ship Research and Development Center Report DTNSDRC-86/047*, May 1986

[9]Uberoi, M.S., and Kovasznay, L.S.G., "On Mapping and Measurement of Random Fields," *Quart. Appl. Math.*, **10** (1953) 375-393

[10]Lauchle, G.C., "Effect of Turbulent Boundary Layer Flow on Measurement of Acoustic Pressure and Intensity," *Noise Control Engr. J.*, **23** Sep-Oct (1984) 52-59

[11]Howe, M.S., "Surface Pressures and Sound Produced by Turbulent Flow Over Smooth and Rough Walls," *J. Acoust. Soc. Amer.*, **90** (2) (1991) 1041-1047

[12]Chase, D.M., "Modeling the Wavevector-Frequency Spectrum of Turbulent Boundary Layer Wall Pressure," *J. Sound Vibration.*, **70** (1) (1980) 29-67

[13]Bendat, J.S., and Piersol, A.G., *Random Data Analysis and Measurement Procedures*, 2nd Edition, John Wiley and Sons Inc., 1986

[14]Bull, M. K., "Wall-Pressure Fluctuations Associated with Subsonic Turbulent Boundary Layer Flow," *J. Fluid Mech.*, **(28)** (1967) 719-754

[15]Chase, D. M., "The Character of the Turbulent Wall Pressure Spectrum at Subconvective Wavenumbers and a Suggested Comprehensive Model," *J. Sound Vib.*, **(112)**(1) (1987) 125-147

[16]Martin, N.C., and Leehey, P., "Low wavenumber Wall Pressure Measurements Using a Rectangular Membrane as a Spatial Filter," *J. Sound Vib.*, **(52)** (1977) 95-120

[17]Lauchle, G. C., and Daniels, M. A., "Wall-Pressure Fluctuations in Turbulent Pipe Flow," *Phys. Fluids A*, **(30)** (10) (1987) 3019-3024

[18]Horne, M. P. and Handler, R. A., "Note on the Cancellation of Contaminating Noise in the Measurement of Turbulent Wall Pressure Fluctuations," *Experiments in Fluids*, **(12)** (1991) 136-139

[19]Schewe, G., "On the Structure and Resolution of Wall-Pressure Fluctuations Associated with Turbulent Boundary-Layer Flow," *J. Fluid Mech.*, **(134)** (1983) 311-328

[20]McCormick, J.W., and Salvadori, M.G., *Numerical Methods in FORTRAN*, Prentice Hall Publications, 1965

[21]McEachern, J.F., and Lauchle, G.C., "A Study of Flow Induced Noise on a Bluff Body," *NCA-Vol. 13- Structure and Flow Sound Interactions*, eds. T.M. Farabee and M.P. Paidoussis, ASME Book No. G00724, (1992) 23-38

[22]Farabee, T.M., and Casarella, M.J., "Spectral Features of Wall-Pressure Fluctuations Beneath Turbulent Boundary Layers," *Phys. Fluids A*,**(3)** (10) (1991) 2410-2420

Appendix A

PLOTS OF WAVEVECTOR-FREQUENCY SPECTRUM

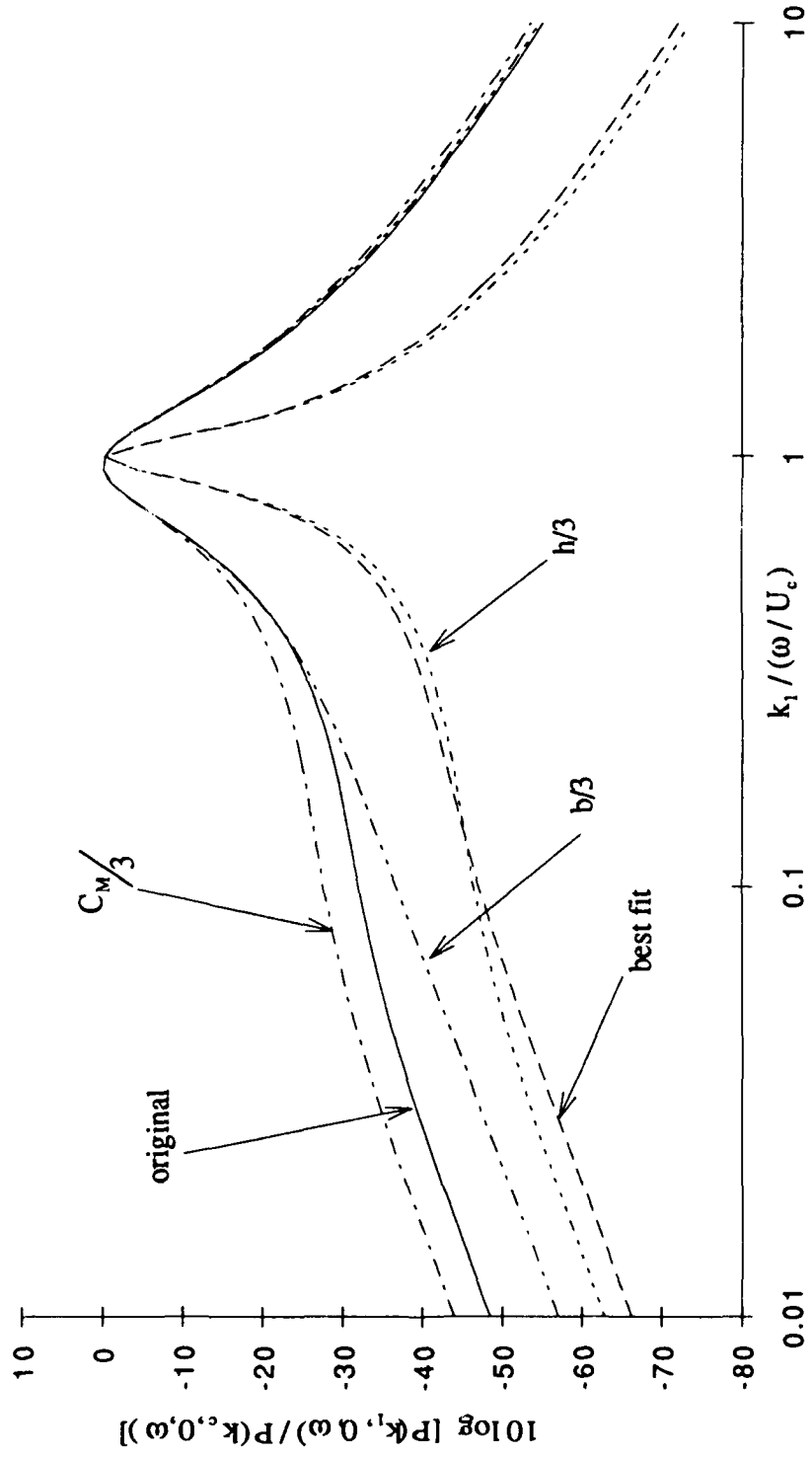

Figure A1 - Wavevector Frequency Spectrum from 1987 Compressible Model for Glycerine Flow Parameters at Frequency=100 Hz

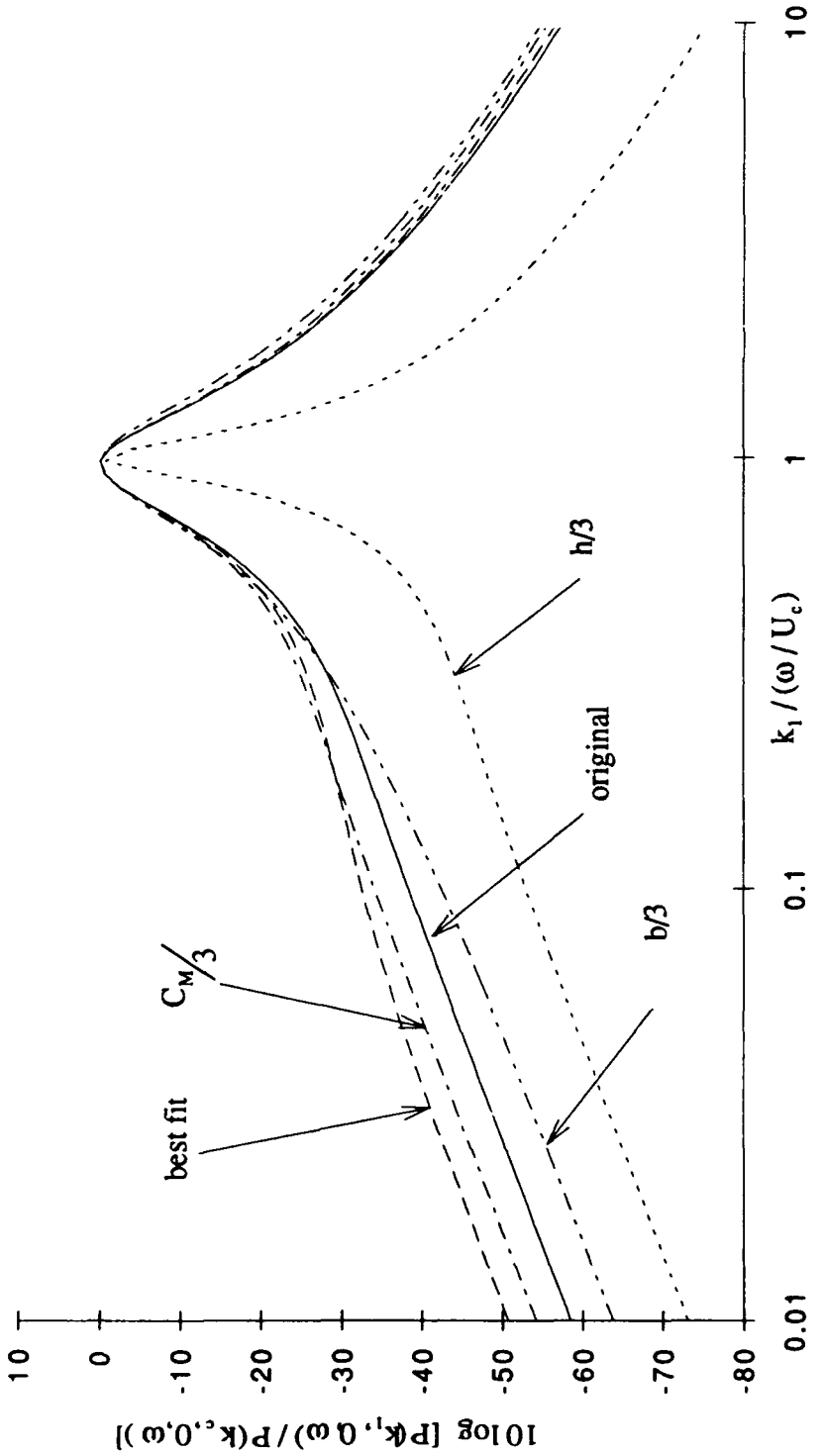

Figure A2 - Wavevector Frequency Spectrum from 1987 Compressible Model for Water Flow Parameters at Frequency=100 Hz

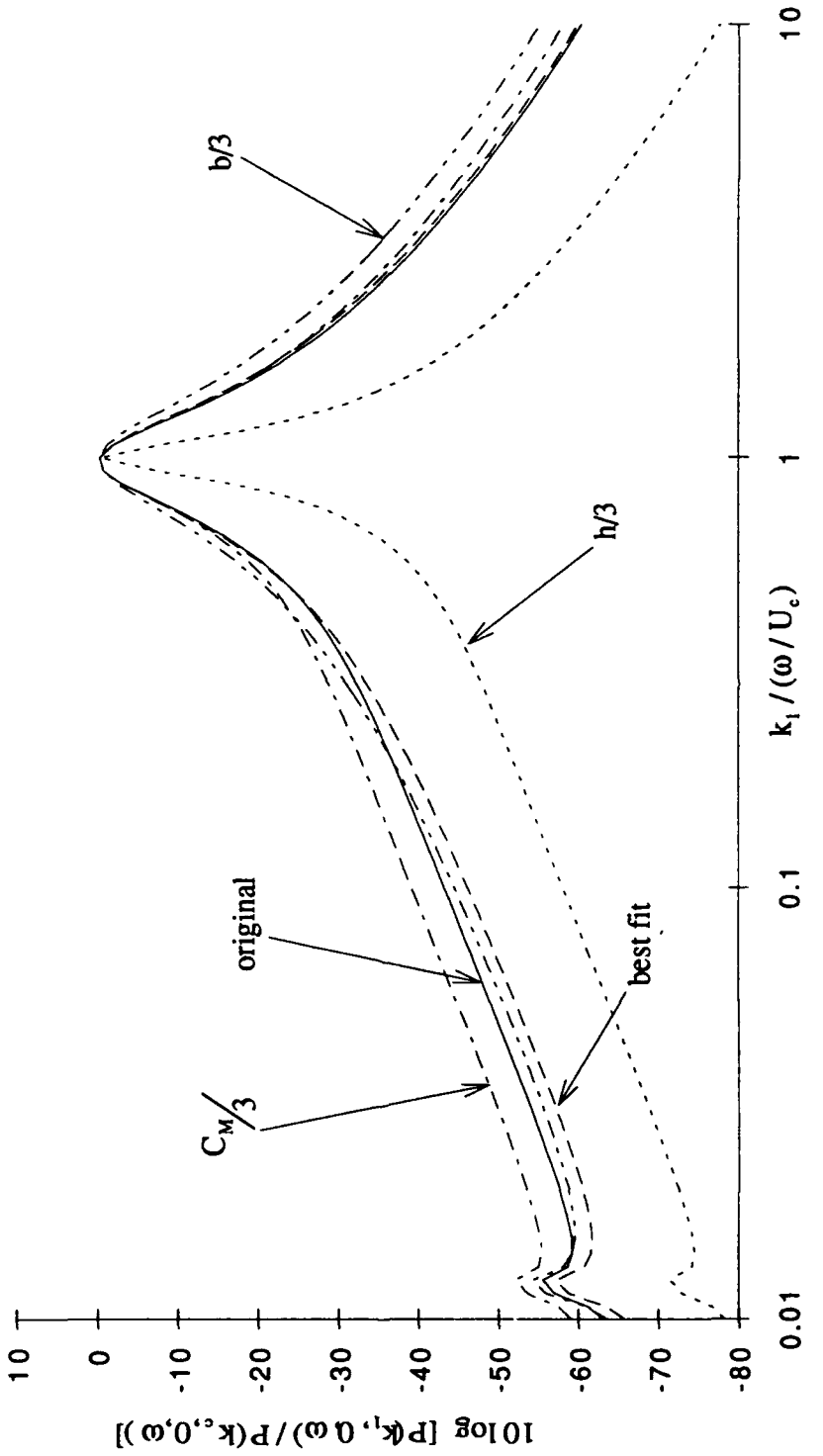

Figure A3 - Wavevector Frequency Spectrum from 1987 Compressible Model for Air Flow Parameters at Frequency=100 Hz

Appendix B

MATLAB COMPUTER PROGRAM TO CALCULATE TURBULENT BOUNDARY LAYER WALL PRESSURE SPECTRUM USING CHASE'S 1987 COMPRESSIBLE MODEL

```
%This program calculates the turbulent boundary layer wall pressure spectrum by
%integrating the wavenumber frequency spectrum given by by D.M. Chase in his
%1987 paper. The program is different from Chase's 1980 model in two ways:
%the values of the constants Cm and Ct, and Pt is multiplied by a term called mod.
%This program uses Eqn (40)from Chase's 1987 paper-the compressible form
%of the wall pressure spectrum model. This takes the incompressible form
%developed by Chase in the 1987 program and multiplies Cm and Ct by factors
%to account for compressiblity in the acoustic wavenumber domain.

%Note: For air calculations, vstar is given.
%For glycerine and water vstar comes from calculated wall shear stress.

clear
t=clock;
flops(0);                                   %timer for calculations

%Re=10890.0;                                %Re for Lauchle glcerine exp
%rho=1238.0;                                %density glycerine kg/m^3 at 35 degress C
%U=7.15;                                    %free stream velocity in m/s glycerine
%r=.00025;                                  %radius of sensor in m for glycerine exp
%nu=.000172;                                %kinematic viscosity in m^2/s
%rad=.14;                                   %pipe radius in meters
%delta=0.14;                                %delta glycerine exp in meter
%Tauw=.03325*rho*U^(7/4)*nu^(1/4)*rad^(-1/4);      %Wall shear stress for pipe
%c=1980;                                    %speed of sound in glycerine m/s

%Re=25000.0;                                %Re for NRL water exp
%rho=998.0;                                 %density water kg/m^3 for water 20 degrees C
%U=1.7;                                     %free stream velocity for NRL water
%r=.00025;                                  %radius of sensor in m for NRL exp
%nu=.000001005;                             %kinematic viscosity in m^2/s
%rad=.0125;                                 %pipe radius in meters
%delta=.0125;                               %delta water exp in meter
%c=1481;                                    %speed of sound in water m/s
%Tauw=.03325*rho*U^(7/4)*nu^(1/4)*rad^(-1/4);      %Wall shear stress for pipe

rho=1.20;                                   %density air in kg/m^3-0 degrees C
U=6.3;                                      %freee stream velocity air for Schewe
delta=.03;                                  %boundary layer thickness Schewe
Tauw=.09;                                   %wall shear stress given by Schewe (Pa)
r=.0005;                                    %radius of sensor in m for Schewe exp
c=343;                                      %speed of sound in air m/s
vstar=.273;                                 %friction velocity m/s
%When calculating in air change conversion to 20 micro Pa at bottom of program


%Tauw=.029*rho*U^2.0*Re^(-0.2);             %wall shear stress for flat plate
Uc=U.*0.65;                                 %convective velovity is .65*free stream
%vstar=(Tauw./rho)^0.5;                     %friction velocity
```

```
%B=0.75;                                % calculated constants
%mu=0.176;
%H=(mu.*Uc)./vstar;
%Ct=.014/H;
%Cm=.466/H;

H=3.0;                                  %constants from Chase 1987
Ct=.0047;
Cm=.1553;
B=.25;
c2=0.1667;
c3=0.1667;


size=30.0;                              %number of freq pts in log increments

kc=zeros(1,size);                       %initialize arrays
Gtt=zeros(1,size);
Gtt2=zeros(1,size);
Gtt3=zeros(1,size);
Gtt4=zeros(1,size);
Gtt=zeros(1,size);
data=zeros(1,size);
w=zeros(1,size);
freq=zeros(1,size);


for i=1:size;                           %frequency loop


    w(i)=125.66*(12566.37/125.66)^((i-1)/29);     %frequency span in air
    %w(i)=1.2566*(12566.37/1.2566)^((i-1)/29);    %frequency span in water
    %w(i)=6.2832*(6283.19/6.2832)^((i-1)/29);     %frequency span in glycerine


    kc(i)=w(i)./Uc;                     %convective wavenumber
    a1=-10.1 .*kc(i);
    b1=10.0 .*kc(i);
    a2=-10.1 .*kc(i);                   %lower limit of integration
    b2=10.0 .*kc(i);                    %upper limit of integration

%perform double integration with Simpson's Rule
%Double integration for simpson's rule consists  of fcn evaluated at nine locations.

    nummx=40;                           %number of cells in x & y direction
    nummy=40;


    nx=2.0*nummx;                       %number of points in x & y per cell
    ny=2.0*nummy;
```

```
h=(b1-a1)./nx;                          %step size
h2=(b2-a2)./ny



sum=0.0;
k11=a1;
k12=k11+h;
k13=k12+h;


for j=1:nummx
    k31=a2;
    k32=k31+h2;
    k33=k32+h2;

%calculate componetns of Gtt

%1st location

        Ksq=k11.^2+k31.^2;
        Kcsq=abs((Ksq-w(i)^2./c^2));            %compressibility


  com1=c2*(Kcsq/Ksq)+c3*(Ksq/Kcsq)+1-c2-c3;      %compress. factor for Ct
  com2=Ksq/Kcsq;                                %compress. factor for Cm


   kr=(Ksq.^0.5).*r;                    %calculate hydrophone response fcn

d1=bessel(1,kr);
hyd=((2 .*d1)./kr).^2.0;
kplus=(w(i)-Uc.*k11).^2/(H^2. *vstar^2)+Ksq;
mod=(kplus+(B*delta).^(-2))./   (Ksq+(B*delta).^(-2));
Km=(((w(i)-Uc.*k11).^2/(H^2*vstar^2))+Ksq+(B*delta).^(-2));
Kt=(((w(i)-Uc.*k11).^2/(H^2*vstar^2))+Ksq+(B*delta).^(-2));
phi=rho^2*vstar^3.*(com2*Cm *k11^2 *Km^(-2.5)+com1*Ct*Ksq *mod *Kt.^(-2.5));
f1=phi*hyd;

%2nd location

      Ksq=k12.^2+k31.^2;
      Kcsq=abs((Ksq-w(i)^2./c^2));          %compressibility

com1=c2*(Kcsq/Ksq)+c3*(Ksq/Kcsq)+1-c2-c3;    %compress. factor for Ct
  com2=Ksq/Kcsq;
  %compress. factor for Cm

kr=(Ksq.^0.5).*r;
```

```
d1=bessel(1,kr);
hyd=((2 .*d1)./kr).^2.0;
kplus=(w(i)-Uc.*k12).^2/(H^2. *vstar^2)+Ksq;
mod=(kplus+(B*delta).^(-2))./   (Ksq+(B*delta).^(-2));
Km=(((w(i)-Uc.*k12).^2/(H^2*vstar^2))+Ksq+(B*delta).^(-2));
Kt=(((w(i)-Uc.*k12).^2/(H^2*vstar^2))+Ksq+(B*delta).^(-2));
phi=rho^2*vstar^3.*(com2*Cm *k12^2 *Km^(-2.5)+com1*Ct*Ksq *mod *Kt.^(-2.5));
f2=phi*hyd;

%3rd location

        Ksq=k13.^2+k31.^2;
        Kcsq=abs((Ksq-w(i)^2./c^2));                    %compressibility

  com1=c2*(Kcsq/Ksq)+c3*(Ksq/Kcsq)+1-c2-c3;             %compress. factor for Ct
  com2=Ksq/Kcsq;
  %compress. factor for Cm



kr=(Ksq.^0.5).*r;
d1=bessel(1,kr);
hyd=((2 .*d1)./kr).^2.0;
kplus=(w(i)-Uc.*k13).^2/(H^2. *vstar^2)+Ksq;
mod=(kplus+(B*delta).^(-2))./   (Ksq+(B*delta).^(-2));
Km=(((w(i)-Uc.*k13).^2/(H^2*vstar^2))+Ksq+(B*delta).^(-2));
Kt=(((w(i)-Uc.*k13).^2/(H^2*vstar^2))+Ksq+(B*delta).^(-2));
phi=rho^2*vstar^3.*(com2*Cm *k13.^2 *Km^(-2.5)+com1*Ct*Ksq *mod *Kt.^(-2.5));
f3=phi*hyd;

for k=1:nummy

%4th location

    Ksq=k11.^2+k32.^2;
    Kcsq=abs((Ksq-w(i)^2./c^2));                    %compressibility

  com1=c2*(Kcsq/Ksq)+c3*(Ksq/Kcsq)+1-c2-c3;             %compress. factor for Ct
  com2=Ksq/Kcsq;
  %compress. factor for Cm


kr=(Ksq.^0.5).*r;
d1=bessel(1,kr);
hyd=((2 .*d1)./kr).^2.0;
kplus=(w(i)-Uc.*k11).^2/(H^2. *vstar^2)+Ksq;
mod=(kplus+(B*delta).^(-2))./   (Ksq+(B*delta).^(-2));
Km=(((w(i)-Uc.*k11).^2/(H^2*vstar^2))+Ksq+(B*delta).^(-2));
Kt=(((w(i)-Uc.*k11).^2/(H^2*vstar^2))+Ksq+(B*delta).^(-2));
phi=rho^2*vstar^3.*(com2*Cm *k11^2 *Km^(-2.5)+com1*Ct*Ksq *mod *Kt.^(-2.5));
f4=phi*hyd;
```

```
%5th location

      Ksq=k12.^2+k32.^2;
      Kcsq=abs((Ksq-w(i)^2./c^2));                    %compressibility

  com1=c2*(Kcsq/Ksq)+c3*(Ksq/Kcsq)+1-c2-c3;           %compress. factor for Ct
  com2=Ksq/Kcsq;
  %compress. factor for Cm


kr=(Ksq.^0.5).*r;
d1=bessel(1,kr);
hyd=((2 .*d1)./kr).^2.0;
kplus=(w(i)-Uc.*k12).^2/(H^2. *vstar^2)+Ksq;
mod=(kplus+(B*delta).^(-2))./    (Ksq+(B*delta).^(-2));
Km=(((w(i)-Uc.*k12).^2/(H^2*vstar^2))+Ksq+(B*delta).^(-2));
Kt=(((w(i)-Uc.*k12).^2/(H^2*vstar^2))+Ksq+(B*delta).^(-2));
phi=rho^2*vstar^3.*(com2*Cm*k12.^2 *Km.^(-2.5)+com1*Ct*Ksq *mod *Kt^(-2.5));
f5=phi*hyd;

%6th location

        Ksq=k13.^2+k32.^2;
        Kcsq=abs((Ksq-w(i)^2./c^2));                  %compressibility

  com1=c2*(Kcsq/Ksq)+c3*(Ksq/Kcsq)+1-c2-c3;           %compress. factor for Ct
  com2=Ksq/Kcsq;
  %compress. factor for Cm


kr=(Ksq^0.5).*r;
d1=bessel(1,kr);
hyd=((2 .*d1)./kr).^2.0;
kplus=(w(i)-Uc.*k13).^2/(H^2. *vstar^2)+Ksq;
mod=(kplus+(B*delta).^(-2))./    (Ksq+(B*delta).^(-2));
Km=(((w(i)-Uc.*k13).^2/(H^2*vstar^2))+Ksq+(B*delta).^(-2));
Kt=(((w(i)-Uc.*k13).^2/(H^2*vstar^2))+Ksq+(B*delta).^(-2));
phi=rho^2*vstar^3.*(com2*Cm *k13^2 *Km^(-2.5)+com1*Ct*Ksq*mod *Kt^(-2.5));
f6=phi*hyd;

%7th location

        Ksq=k11.^2+k33.^2;
        Kcsq=abs((Ksq-w(i)^2./c^2));                  %compressibility

  com1=c2*(Kcsq/Ksq)+c3*(Ksq/Kcsq)+1-c2-c3;           %compress. factor for Ct
  com2=Ksq/Kcsq;
  %compress. factor for Cm
```

```
kr=(Ksq.^0.5).*r;
d1=bessel(1,kr);
hyd=((2 .*d1)./kr).^2.0;
kplus=(w(i)-Uc.*k11).^2/(H^2. *vstar^2)+Ksq;
mod=(kplus+(B*delta).^(-2))./   (Ksq+(B*delta).^(-2));
Km=(((w(i)-Uc.*k11).^2/(H^2*vstar^2))+Ksq+(B*delta).^(-2));
Kt=(((w(i)-Uc.*k11).^2/(H^2*vstar^2))+Ksq+(B*delta).^(-2));
phi=rho^2*vstar^3.*(com2*Cm *k11^2 *Km^(-2.5)+com1*Ct*Ksq *mod *Kt^(-2.5));
f7=phi*hyd;

%8th location

    Ksq=k12.^2+k33.^2;
    Kcsq=abs((Ksq-w(i)^2./c^2));                    %compressibility

  com1=c2*(Kcsq/Ksq)+c3*(Ksq/Kcsq)+1-c2-c3;         %compress. factor for Ct
  com2=Ksq/Kcsq;
  %compress. factor for Cm


kr=(Ksq.^0.5).*r;
d1=bessel(1,kr);
hyd=((2 .*d1)./kr).^2.0;
kplus=(w(i)-Uc.*k12).^2/(H^2. *vstar^2)+Ksq;
mod=(kplus+(B*delta).^(-2))./   (Ksq+(B*delta).^(-2));
Km=(((w(i)-Uc.*k12).^2/(H^2*vstar^2))+Ksq+(B*delta).^(-2));
Kt=(((w(i)-Uc.*k12).^2/(H^2*vstar^2))+Ksq+(B*delta).^(-2));
phi=rho^2*vstar^3.*(com2*Cm*k12^2 *Km^(-2.5)+com1*Ct*Ksq*mod*Kt.^(-2.5));
f8=phi*hyd;

%9th location

      Ksq=k13.^2+k33.^2;                            %compressibility


  com1=c2*(Kcsq/Ksq)+c3*(Ksq/Kcsq)+1-c2-c3;         %compress. factor for Ct
  com2=Ksq/Kcsq;
  %compress. factor for Cm


kr=(Ksq.^0.5).*r;
d1=bessel(1,kr);
hyd=((2 .*d1)./kr).^2.0;
kplus=(w(i)-Uc.*k13).^2/(H^2. *vstar^2)+Ksq;
mod=(kplus+(B*delta).^(-2))./   (Ksq+(B*delta).^(-2));
Km=(((w(i)-Uc.*k13).^2/(H^2*vstar^2))+Ksq+(B*delta).^(-2));
Kt=(((w(i)-Uc.*k13).^2/(H^2*vstar^2))+Ksq+(B*delta).^(-2));
phi=rho^2*vstar^3.*(com2*Cm *k13^2 *Km^(-2.5)+com1*Ct*Ksq*mod*Kt^(-2.5));
f9=phi*hyd;

%sum components of molecule
```

```
        sum=sum+(h*h2./9.0).*(f1+f3+f7+f9+4.0 .*(f2+f4+f6+f8)+16.0 .*f5);

%move :o next molecule

        f1=f7;
        f2=f8;
        f3=f9;
        k32=k33+h2;
        k33=k32+h2;
        end

    k11=k13;
    k12=k11+h;
    k13=k12+h;
    end

Gtt(i)=2.0 * sum;

end


Gtt2=Gtt*2*pi ./(4*10^(-10));          %convert Gtt from Pa to dB re 20 microPa
%Gtt2=Gtt*2*pi ./(1*10^(-12));         %convert Gtt from Pa to dB re 1 microPa
Gtt3=10.0 .*log10(Gtt2);
freq=w ./6.28;

semilogx(freq,Gtt3)
freq1=freq';
Gtt4=Gtt3';
save freq freq1 /ascii
save data Gtt4 /ascii
etime(clock,t)
flops
```